Research Article

Structural and biochemical evaluation of bisubstrate inhibitors of protein arginine N-methyltransferases PRMT1 and CARM1 (PRMT4)

Emma A. Gunnell[1,2], Alaa Al-Noori[1,2], Usama Muhsen[1,*], Clare C. Davies[3], James Dowden[1] and Ingrid Dreveny[2]

[1]School of Chemistry, University of Nottingham, Nottingham NG7 2RD, U.K.; [2]Centre for Biomolecular Sciences, School of Pharmacy, University of Nottingham, Nottingham NG7 2RD, U.K.; [3]College of Medical and Dental Sciences, University of Birmingham, Edgbaston, Birmingham B15 2TT, U.K.

Correspondence: Ingrid Dreveny (ingrid.dreveny@nottingham.ac.uk) or James Dowden (james.dowden@nottingham.ac.uk)

Attenuating the function of protein arginine methyltransferases (PRMTs) is an objective for the investigation and treatment of several diseases including cardiovascular disease and cancer. Bisubstrate inhibitors that simultaneously target binding sites for arginine substrate and the cofactor (S-adenosylmethionine (SAM)) have potential utility, but structural information on their binding is required for their development. Evaluation of bisubstrate inhibitors featuring an isosteric guanidine replacement with two prominent enzymes PRMT1 and CARM1 (PRMT4) by isothermal titration calorimetry (ITC), activity assays and crystallography are reported. Key findings are that 2-aminopyridine is a viable replacement for guanidine, providing an inhibitor that binds more strongly to CARM1 than PRMT1. Moreover, a residue around the active site that differs between CARM1 (Asn-265) and PRMT1 (Tyr-160) is identified that affects the side chain conformation of the catalytically important neighbouring glutamate in the crystal structures. Mutagenesis data supports its contribution to the difference in binding observed for this inhibitor. Structures of CARM1 in complex with a range of seven inhibitors reveal the binding modes and show that inhibitors with an amino acid terminus adopt a single conformation whereas the electron density for equivalent amine-bearing inhibitors is consistent with preferential binding in two conformations. These findings inform the molecular basis of CARM1 ligand binding and identify differences between CARM1 and PRMT1 that can inform drug discovery efforts.

Introduction

Protein arginine methyltransferases (PRMTs, E.C. 2.1.1.125) catalyse the transfer of methyl groups from S-adenosylmethionine (SAM) to arginine residues of target proteins, giving a pattern of nitrogen methylations dictated by enzyme type (Figure 1A). Hydrogen bonding N-H moieties are replaced by hydrophobic N-methyl groups to effect protein–protein interactions as a result. Co-activator associated arginine methyltransferase (CARM1, or PRMT4) targets substrates that contain proline-rich sequences rather, than the GGRGG sequences favoured by PRMT1. PRMTs are involved in the regulation of numerous cellular processes including chromatin function [1–8], RNA processing [9,10], and DNA-damage response [11–13]. Co-activation of gene transcription is effected by methylation of histone arginines: H4R3 by PRMT1; or H3R17 and H3R26 by CARM1, for example. Meanwhile, methylation of RNA binding proteins is involved in the regulation of protein translation. An increasing body of evidence links PRMT dysregulation to disease processes, including asthma, kidney and cardiovascular disease and cancer [14–17], underlining the need for potent, well-characterised PRMT inhibitors as molecular probes and potential therapeutic agents. CARM1 is overexpressed in breast [18], prostate [19], lung [20], liver [21], and colorectal cancer [22]. CARM1 inhibition has been shown to slow tumour growth in a multiple myeloma xenograft model [23], inhibit liver cancer
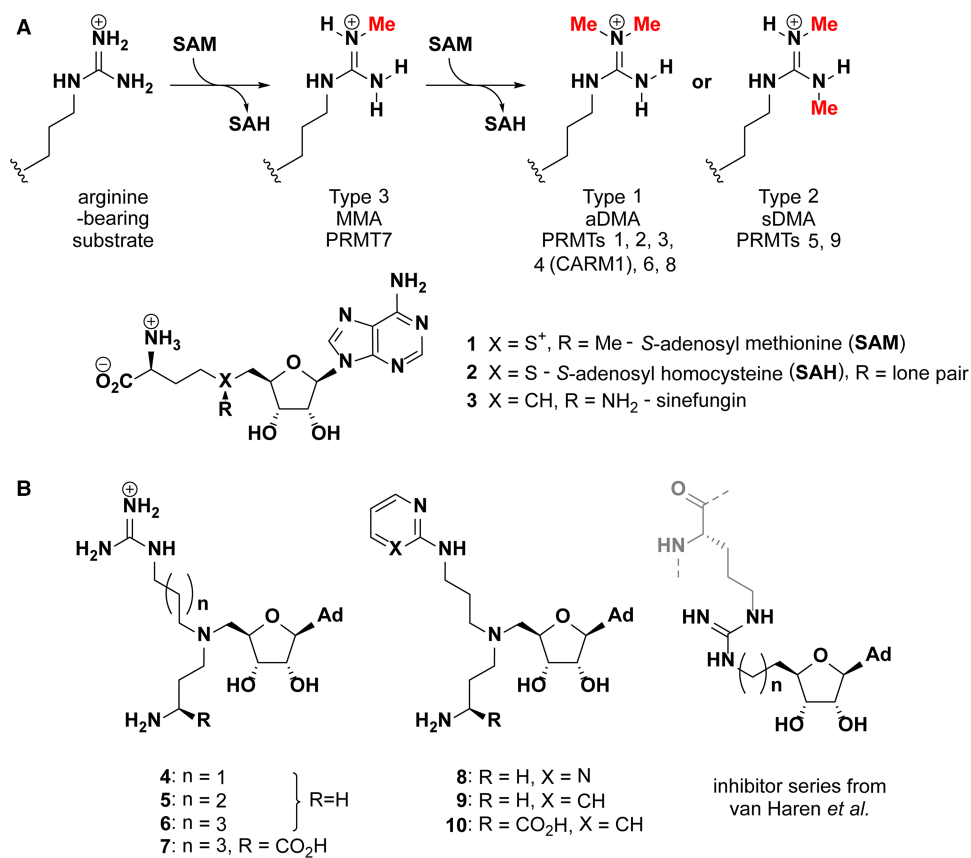
Figure 1. PRMT classification and inhibitor structures.

(**A**) Arginine methylation patterns deposited by PRMTs. The PRMTs are classified as type 1, 2 or 3 according to whether they generate monomethylarginine (MMA), symmetric dimethyl arginine (sDMA) or asymmetric dimethylarginine (aDMA); (**B**) Structures of bisubstrate azo-SAM inhibitors from the present study (**4–10**) and those reported previously by van Haren et al. [28,33].

cell proliferation [21] and impair AML initiation and proliferation [24]. PRMT1 on the other hand catalyses the majority of methylation events in the cell and is overexpressed in breast cancers, prostate cancers, and leukemia [15].

PRMT inhibitors reported to date can be broadly categorised into SAM analogues (including the pan-methyltransferase inhibitors sinefungin (**3**) and *S*-adenosyl homocysteine (**2**), (Figure 1A)), substrate peptide analogues [25–28], and structures optimised from high throughput screening hits [29–32]. Promising CARM1 inhibitors include EPZ022302/EZM2302 (a 6 nM CARM1 inhibitor with anti-tumour activity *in vivo*) [23] and TP-064 (IC$_{50}$ < 10 nM against CARM1 and >100-fold selective over other methyltransferases) [32]. In both cases, ternary crystal structures with CARM1-SAH showed the inhibitor to occupy the substrate-binding pocket with kinetic data supporting noncompetitive inhibition with respect to both SAM and peptide substrate [23,32]. Alternatively, inhibitors may occupy both the SAM and arginine binding sites (Figure 1B) [28,33–35]. A number of such inhibitors that target CARM1 feature amino adenosine linked to modified cytosine moieties that occupy the SAM and arginine binding site, respectively [36]. The most potent of these inhibitors displayed an IC$_{50}$ of 1.5 µM against CARM1, and was 100-fold less potent against PRMT1. Design of selective inhibitors is challenging however, since the residues involved in SAM and substrate arginine binding are largely conserved in the nine PRMTs encoded in the human genome, particularly between type I family members [37]. In line with recent advances [38], the development and structural investigation of rationally designed bisubstrate inhibitors remains a desirable route to identify individual residue variations that may contribute to selective inhibition of CARM1 over PRMT1 for example.

Bisubstrate inhibitors featuring guanidinium and aza-adenosylmethionine moieties joined by alkyl linkers were previously reported. Longer linkers appeared to confer a degree of selectivity between CARM1 and PRMT1, which was rationalised based on docking studies [34]. Van Haren et al. have also explored this approach by 5′-hydroxyl group of adenosine with a methylguanidinium group, which resulted in a compound with 100-fold selectivity for CARM1 over PRMT1 [33]. Extending the guanidinium group to a CARM1 substrate peptide achieved a greater degree of selectivity for CARM1 over PRMT1 (IC_{50} values of 0.09 and 25.5 μM, respectively for the most selective compound) [28]. Whilst promising in their apparent selectivity, a key drawback of such peptide-fused mimics is their potential susceptibility to proteolysis, which limits their utility in cellular assays and *in vivo* applications.

Novel non-peptidic bisubstrate inhibitors and crystal structures of their complexes with CARM1 are reported here. Isothermal titration calorimetry and activity assays allowed measurement of affinity and inhibition of both PRMT1 and CARM1. Data herein shows that replacement of the guanidinium group with an aminopyridine or aminopyrimidine enhances the inhibitors' affinity for CARM1 but not PRMT1. The influence of a specific active site residue on the orientation of the catalytic glutamate and inhibitor binding was evaluated with CARM1 N265Y mutant protein; crystal structures revealed that this mutation affects the conformation of key residues at the substrate-binding site.

Experimental procedures

Constructs, protein expression and purification

The catalytic domain of human CARM1, residues 135 to 479 ($CARM1_{135-479}$; isoform 3, UniProt accession code Q86X55) was cloned into the vector pMALX(E) (a modified pMAL-c2x vector, kindly provided by Lars Pederson [39]) using restriction sites *NotI* and *HindIII* with the addition of a C-terminal His-tag and a TEV cleavage site directly upstream of the CARM1 sequence. The final sequence expressed was MBP-AALAAAQT-NAAAAENLYFQ-$CARM1_{135-479}$-HHHHHH. $CARM1_{135-479}$ was expressed in BL21-CodonPlus (DE3)-RIL cells (Agilent) at 20°C after induction with 0.4 mM IPTG. After 20 h, cells were harvested by centrifugation, resuspended in 50 mM Tris, 300 mM NaCl, 20 mM imidazole, 5% v/v glycerol at a pH of 7.5 (buffer A), lysed by sonication, and the lysate clarified by centrifugation. $CARM1_{135-479}$ was purified by nickel affinity chromatography (5 ml HiTrap chelating HP column, GE Healthcare) using buffer A with a gradient elution of 20 to 500 mM imidazole over 20 column volumes. The protein was concentrated to ∼1 mg/ml and cleaved with TEV protease to remove the MBP tag. The cleaved protein was then separated from TEV protease and the MBP tag by gel filtration (HiLoad Superdex S200 16/60 PG, GE Healthcare), fractions containing the protein concentrated and 1 mg/ml aliquots either used directly or flash frozen and stored at −80°C until further use. Approximately 0.2 mg CARM1 catalytic domain was obtained per litre of bacterial culture.

Human PRMT1, residues 22 to 361 ($PRMT1_{22-361}$; isoform 1/splice variant 2, Uniprot accession code Q99873), was cloned into vector pET-26b(+) using restriction sites *NdeI* and *XhoI*. $PRMT1_{22-361}$ was expressed and purified as outlined for CARM1, except that buffers were at pH 8.0 and the His-tagged protein obtained from nickel affinity chromatography was concentrated and loaded directly onto a gel filtration column. Approximately 2 mg of PRMT1 were obtained per litre of bacterial culture.

The sequence for histone peptide H4 residues 1 to 21 (herein referred to as $H4_{1-21}$) and the sequence for histone peptide H3, residues 3–31 (herein referred to as $H3_{3-31}$) were cloned into a modified pET-21a(+) vector containing an N-terminal GB tag and a C-terminal His-tag. $H4_{1-21}$ and $H3_{3-31}$ were expressed and purified as described above for PRMT1 except that the buffers had a lower NaCl concentration of 150 mM. Aliquots of the peptides were concentrated to 400 μM, flash frozen, and stored at −80°C until needed.

Inhibitor compounds

Synthesis of **4** and **7** was described previously [34], **5**, **6**, **8**, **9** and **10** were prepared similarly and are described in the Supplementary Information.

Crystallisation

Co-crystallisations of $CARM1_{135-479}$ with inhibitors were carried out in 24-well plates using the sitting-drop vapour diffusion method. In the case of compound **5**, the CARM1 catalytic domain was concentrated to 1.7 mg/ml, followed by addition of a 500 μM aqueous stock solution of inhibitor such that the final protein concentration was 28 μM and the final ligand concentration was 167 μM. Co-crystallisations were performed

by mixing 1 μl of the protein-inhibitor solution with 1 μl of a solution containing 0.1 M Bis-tris propane-Cl at a pH of 7.0, 0.02 M potassium phosphate and 22% (w/v) PEG 3350 in sitting drop trays. Trays were incubated at 20°C and crystals grew within one week. Co-crystallisations with the other inhibitors were carried out with similar ligand concentrations and temperatures, but the crystallisation conditions, and CARM1 concentrations varied as detailed in Supplementary Table S1. Crystals were cryoprotected in the well solution supplemented with 30% (v/v) glycerol and 20% (w/v) PEG 3350 prior to cryocooling in liquid nitrogen.

Data collection, structure determination and refinement

Datasets were collected at the European Synchrotron Radiation Facility, Grenoble, France or Diamond Light Source, Harwell, Oxford using beamlines I02, ID30B and ID30A-1. Crystals belong to space group $P2_12_12$, with four monomers in the asymmetric unit. All CARM1 structures were solved by molecular replacement using Phaser MR [40]. The structure of CARM1 in complex with sinefungin (**3**) and an inhibitor (PDB code 2Y1X) [41] or subsequently CARM1 in the CARM1–**5** complex structure were used as search models in molecular replacements (with the ligands removed). Model building was carried out in COOT [42] and refinement was carried out with Phenix [43] and Refmac [44]. Ligand restraints were generated using eLBOW [45]. All structural images were generated using The PyMOL Molecular Graphics System, Version 1.8 Schrödinger, LLC. Parameters for data collection, structural refinement and validation are listed in Supplementary Table S2.

Enzymatic assays

Methylation reactions contained $PRMT1_{22–361}$ (160 nM), H4(1–21) (40 μM) and adenosyl-L-methionine, S-[methyl-^{3}H] (PerkinElmer, NET155H250UC) at a final concentration of 0.23 μM, in phosphate buffered saline buffer at pH 7.3 in the presence of the different inhibitors. For IC_{50} curves, a minimum of 10 inhibitor concentrations were used, and experiments were carried out in duplicate. The reactions were initiated by addition of adenosyl-L-methionine, S-[methyl-^{3}H] and incubated at 30°C after mixing. After 60 min, optimised for signal to noise ratio in the linear region, each reaction mixture was transferred by pipette onto a P81 phosphocellulose paper square (PerkinElmer) and immediately immersed in a stirred solution of trichloroacetic acid (10% w/v). The phosphocellulose squares were washed for 3×10 min, replacing the 10% trichloroacetic acid after each wash. A final wash was carried out with 95% ethanol, the squares removed and allowed to dry. Incorporation of tritium into the histone substrate was determined by liquid scintillation counting. For each inhibition series, a no-substrate control reaction was included, which contained water in place of the histone substrate. This data point was included in the data used to fit the curve by setting the x-value (log[I]) to 4.0. A no-inhibitor control was also included in the data, with the x-value (log[I]) set to -3.0. These control samples were also run in duplicate.

CARM1 methylation reactions were carried out using 0.23 μM adenosyl-L-methionine, S-[methyl-^{3}H], 320 nM $CARM1_{135–479}$ and 120 μM histone substrate (H3(3–31)). Since CARM1 automethylates, a no-enzyme control was used as the maximum inhibition sample (log[I] set to 4.0). Data were analysed in GraphPad Prism 7 and fit using non-linear regression using the 'log(inhibitor) vs. response — variable slope (four parameters)' function with no constraints. The concentrations of inhibitor solutions were determined using a NanoDrop 1000 v3.7, using the molar extinction coefficient at 260 nm for S-adenosyl homocysteine ($\varepsilon = 15\,400$ M^{-1} cm^{-1}). 2-alkylaminopyrimidines (**8**) and 2-alkylaminopyridines (**9** and **10**) absorb at 260 nm with extinction coefficients of $<15\,400$ M^{-1} cm^{-1} [46,47]. The concentrations of **8**, **9** and **10** may therefore have been overestimated by up to two-fold with corresponding effect on the estimated K_d and IC_{50} values for these inhibitors.

Isothermal titration calorimetry (ITC)

Titrations were carried out using a MicroCal PEAQ-ITC Isothermal Titration Calorimeter (Malvern) or MicroCal iTC200 (Malvern) in the case of the titration of **5** into $PRMT1_{22–361}$. Data analysis was carried out using MicroCal PEAQ-ITC Analysis Software. Inhibitors were dissolved in gel filtration buffer to concentrations between 150 and 736 μM as suitable for ITC assays. An amount of 2.4 μl injections of inhibitor solutions into the protein solution at concentrations between 21 and 121 μM were performed, at 25°C. Control titrations were carried out by titrating the inhibitor solution into the buffer solution. The control heats of dilution were subtracted from binding experiments prior to curve fitting using a one-site binding model with fitted offset. The raw data and integrated fitted curves are shown in Supplementary Figures S2, S4, S6–S8 derived thermodynamic parameters are listed in Supplementary Tables S3, S4. Protein concentrations were determined by UV absorbance at 280 nm (with a NanoDrop 1000 v3.7) using extinction coefficients at 280 nm determined by the ExPASy ProtParam online tool. The protein concentrations calculated in this manner were shown to be in
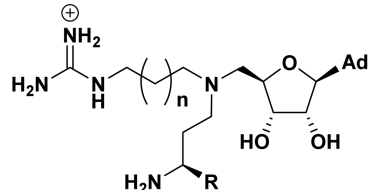
good agreement with the concentration determined by Bradford assay using a BSA standard. Inhibitor concentrations were determined as for activity assays. In two instances (**7** into PRMT1 and **10** into CARM1 N265Y), low c-value curves necessitated fixing the stoichiometry prior to curve-fitting.

Results

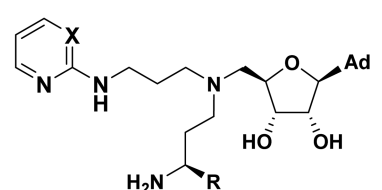## Inhibitors of both PRMT1 and CARM1 that bind in a bisubstrate manner

Putative bisubstrate inhibitors **4**, **5** and **6** containing amines and arginine-mimicking alkylguanidinium groups with chain lengths increasing from three to five methylenes respectively (Figure 1B) were assessed for their potential to bind and inhibit CARM1 and PRMT1. A radiometric methylation assay was used to assess the inhibitory strength of this series of inhibitors (Supplementary Figure S1) and resulting IC_{50} values are shown in Table 1, entries 1–3. Comparison of IC_{50} values for inhibitors **4**–**6** revealed a modest decrease in potency (2.3 to 17.7 μM) against $CARM1_{135-479}$ as the length of the alkyl linker between the aminoadenosine and guanidinium groups is increased from 3 to 5 methylene units. No such trend was observed for PRMT1, with inhibitors displaying similar IC_{50} values for $PRMT1_{22-361}$ (7.2–11.8 μM) as CARM1. Isothermal titration calorimetry was then used to determine the dissociation constants of this inhibitor series for PRMT1 and CARM1 (Table 1; Supplementary Figure S2; Supplementary Table S3). The resultant K_d values showed a similar pattern to the IC_{50} values, with all inhibitors binding with low micromolar affinity to both PRMT1 and CARM1 and again, CARM1 displayed a slight preference for a shorter alkyl linker length (Table 1). Inhibitor **7** (the amino acid analogue of **6**), was also evaluated and found to bind and inhibit both PRMT1 and CARM1 to a similar extent (Table 1; Supplementary Figure S2; Supplementary Table S3).

Table 1 K_d and IC_{50} values for series of inhibitors (4–10) and SAH against PRMT1 and CARM1 measured using ITC and enzyme activity assays, respectively

4: n = 1
5: n = 2 } R=H
6: n = 3
7: n = 3, R = CO_2H

linker length guanidines

8: R = H, X = N
9: R = H, X = CH
10: R = CO_2H, X = CH

3C aromatic isosteres

Inhibitor	K_d ± standard error (μM)		IC_{50} (95% confidence interval) (μM)	
	PRMT1	CARM1	PRMT1	CARM1
4	10.2 ± 0.996	3.32 ± 0.335	7.2 (3.5–15.0)	2.3 (1.8–3.0)
5	4.02 ± 0.453	7.18 ± 0.557	11.8 (9.0–15.5)	8.7 (6.9–10.8)
6	9.99 ± 1.89	9.80 ± 1.83	11.6 (4.9–27.2)	17.7 (13.5–23.2)
7	32.2 ± 3.53[1]	38.1 ± 9.61	22.0 (14.4–33.5)	24.1 (15.4–37.6)
8	10.2 ± 4.21	2.30 ± 0.162	22.0 (15.7–30.8)	0.7 (0.5–1.0)
9	15.3 ± 1.57	1.14 ± 0.411	11.1 (5.6–21.8)	0.3 (0.1–1.1)
10	43.7 ± 14.9[2]	1.11 ± 0.132	25.3 (17.3–37.0)	0.8 (0.6–1.0)
SAH	0.709 ± 0.057	0.775 ± 0.111	0.5 (0.2–1.0)	0.2 (0.1–0.4)

[1]Stoichiometry fixed to 0.5.
[2]This K_d is derived from a competition experiment with SAH as the K_d was not accessible through direct titration.

Co-crystallisation trials were carried out with the aim of determining the binding mode and whether the molecules bound as bisubstrate inhibitors. The catalytic core of CARM1 was crystallised in the presence of amine-guanidine inhibitors **4**, **5**, **6** and **7**, and the structures solved by molecular replacement. Crystals belonged to space group P $2_1 2_1 2$ with two CARM1 dimers in the asymmetric unit, in line with CARM1 structures that have been previously reported [23,41,48]. Data collection and refinement statistics are shown in Supplementary Table S2.

Electron density corresponding to each of these respective inhibitors was clearly observed in the active site (Figure 2A–D). Superposition of the CARM1 complex structures with a published structure of CARM1 in complex with SAM-mimic sinefungin (**3**) and a histone 3 tail substrate (PDB code 5DX0 [48]) revealed that
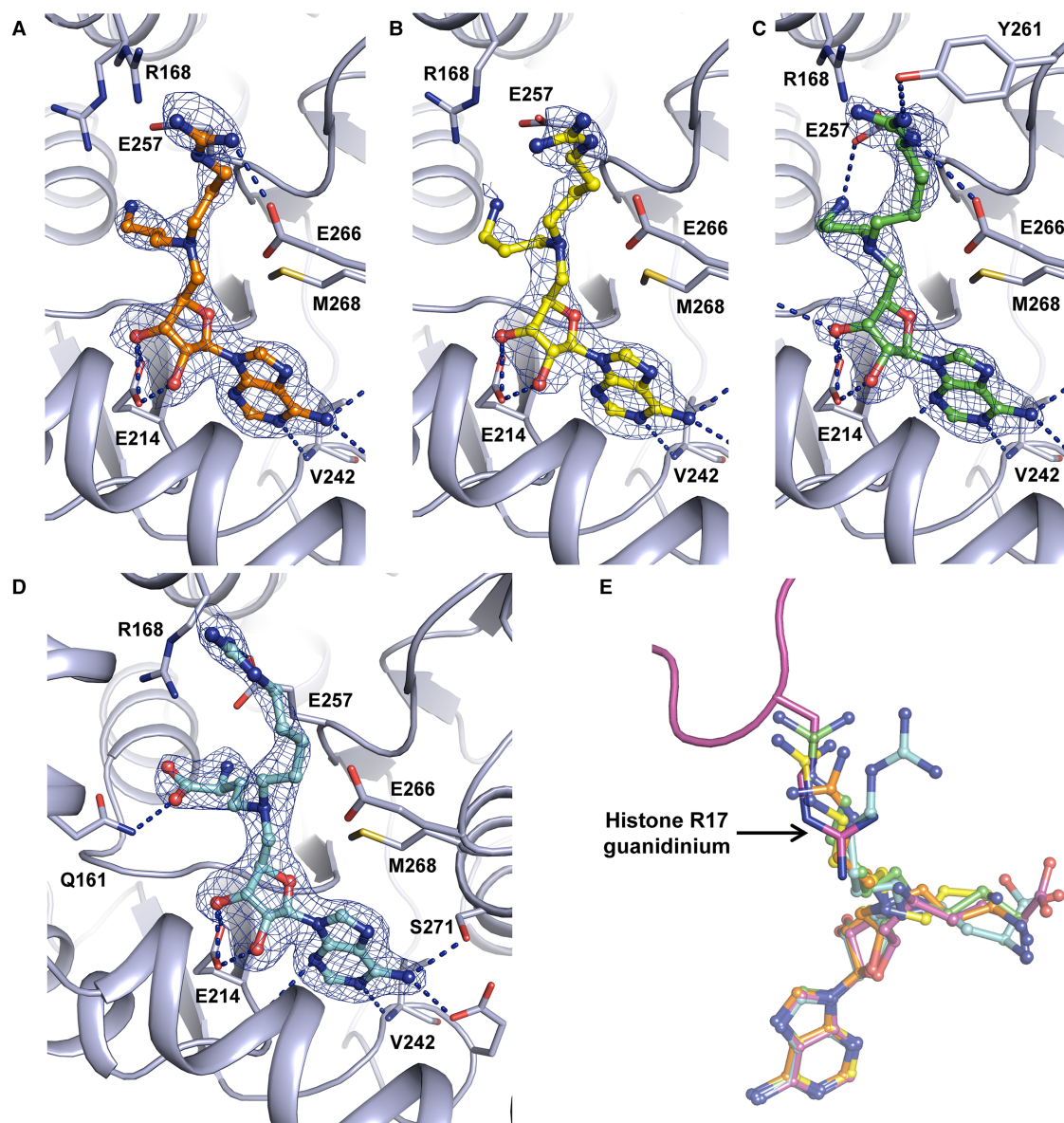

Figure 2. Crystal structures of inhibitors 4, 5, 6 and 7 in complex with CARM1.
(**A–D**) $2mF_o\text{-}DF_c$ electron density maps contoured at $\sigma = 1$ for **4** (a), **5** (b), **6** (c) and **7** (d) in ball-and-stick representation bound in the CARM1 active site. Polar contacts assigned using PyMol are indicated with blue dashed lines and residues involved in SAM and substrate arginine binding (and those involved in putative polar contacts) are shown. (**E**) Superposition of **4** (orange), **5** (yellow), **6** (green) and **7** (cyan) structures as bound to CARM1 with a published structure of CARM1 in complex with histone 3 and sinefungin (magenta, PDB code 5DX0 [48]).

the positions of the adenosine moieties of inhibitors **4–7** in the CARM1 active site closely match that of sine-fungin (Figure 2E). The alkylguanidinium group also extends into the arginine binding channel as designed, confirming the bisubstrate nature of inhibition. In comparison with the position of H3 Arg-17 (the arginine targeted for CARM1 methylation), the guanidinium groups of all inhibitors reach beyond Glu-257 (which forms a bidentate interaction with the substrate arginine η nitrogens) and Glu-266 (that forms a hydrogen bond to the ε nitrogen of substrate arginines) [48]. The B factors of the guanidinium groups of **4**, **5** and **6** and **7** are relatively high compared with the other ligand atoms, which may suggest that this group retains some flexibility when bound in the active site (Supplementary Figure S3).

Substitution of the guanidinium group for a 2-aminopyridine improves binding to CARM1 but not PRMT1

Inhibitors **8**, **9** and **10** (Figure 1B) were synthesised with a view to replacing the guanidinium group with less polar 2-aminopyrimidine (**8**) or 2-aminopyridine (**9**, **10**) isosteres. Binding affinities for these molecules with CARM1 (K_d of 2.30 μM (**8**), 1.14 μM (**9**) and 1.11 μM (**10**), Table 1; Supplementary Figure S4; Supplementary Table S3) were found to be comparable with that obtained for guanidine inhibitor **4** (K_d 3.32 μM). An activity based assay returned IC_{50} values about five-fold lower (0.7 μM (**8**), 0.3 μM (**9**), 0.8 μM (**10**)), than the guanidinium substituted analogue (2.3 μM for **4**), Table 1 and Supplementary Figure S5. The same molecules (**8–10**) were ∼30-fold less potent inhibitors of PRMT1.

To gain insight into the binding mode of these ligands, **8**, **9** and **10** were co-crystallised with CARM1 and the resulting structures solved by molecular replacement. Examination of active site electron density maps showed that in all cases the position of the adenosine moiety was the same as observed earlier in structures of CARM1 in complex with **4–7** (Figure 3A,B). It was apparent that inhibitors **8** and **9** occupy two conformations within the CARM1 active site, in which the amine and aromatic groups alternately occupy the binding channels of the substrate arginine and the SAM amino acid (Figure 3A,D). Interestingly, introduction of a carboxylate group (as in **10**) resulted in a clear preference for one binding pose within the active site (Figure 3B). This may be attributed to an interaction between Arg-168 and the inhibitor carboxylate, which mimics the carboxylate group of SAM. ITC experiments with **10** revealed that introduction of this carboxylate group does not affect the affinity for CARM1 (Table 1; Supplementary Figure S4; Supplementary Table S3).

No binding of **10** to PRMT1 directly (IC_{50} of 25.3 μM) was observed using ITC under the same conditions as for the other inhibitors (Table 1). To exclude the possibility that **10** inhibits PRMT1 through nonspecific destabilisation, SAH (**2**) was titrated into a solution of PRMT1 and **10**. The presence of **10** in the cell resulted in an increase in the apparent K_d of SAH (**2**) for PRMT1, while the stoichiometry remained unchanged (Supplementary Table S4). Fitting the resulting isotherm using a competitive binding model thus provided a $K_d \sim 43.7$ μM estimate of **10** for PRMT1 (Supplementary Figure S6).

CARM1 Asn-265 may contribute to the preferential binding of heteroaromatic inhibitors

To explore differences between the CARM1 and PRMT1 active sites, attention focused on two residues in the CARM1 substrate-arginine binding channel (Figure 4). The first, Asn-161 (Glu-55 in PRMT1), was identified as a possible cause for preferential binding of 5C amino acid/guanidine inhibitor **7** to PRMT1 observed previously [34]. A difference in sequence at position CARM1 Asn-265, which corresponds to Tyr-160 in PRMT1 was identified by analysing structural alignments of PRMT1 and CARM1. We hypothesised that the residue in this position may affect the conformation of neighbouring glutamate Glu-266 (Glu-161 PRMT1), which is critical for orienting the substrate arginine residue for methylation and is in close proximity to the aromatic rings in compounds **9** and **10**. This glutamic acid residue adopts a different conformation in CARM1 compared with PRMT1 crystal structures (Figure 4B,D). CARM1 Asn-265 may therefore affect the Glu-266 conformation and, as a consequence, its interactions with the aromatic rings in compounds **9** and **10**. In order to evaluate the possible effects of these two sequence differences CARM1 residues Asn-161 and Asn-265 were mutated into the corresponding PRMT1 residues, Glu and Tyr located at equivalent positions, respectively (Figure 4).

The mutation CARM1 N161E renders the rim of the substrate arginine binding pocket more like PRMT1. Inhibitors (**8**, **9**, **10** and SAH) showed marginally greater affinity (K_d 0.133–1.11 μM) for the CARM1 N161E mutant compared with wild-type (WT) (0.774–2.30 μM, Table 2; Supplementary Figures S7, S8). The second
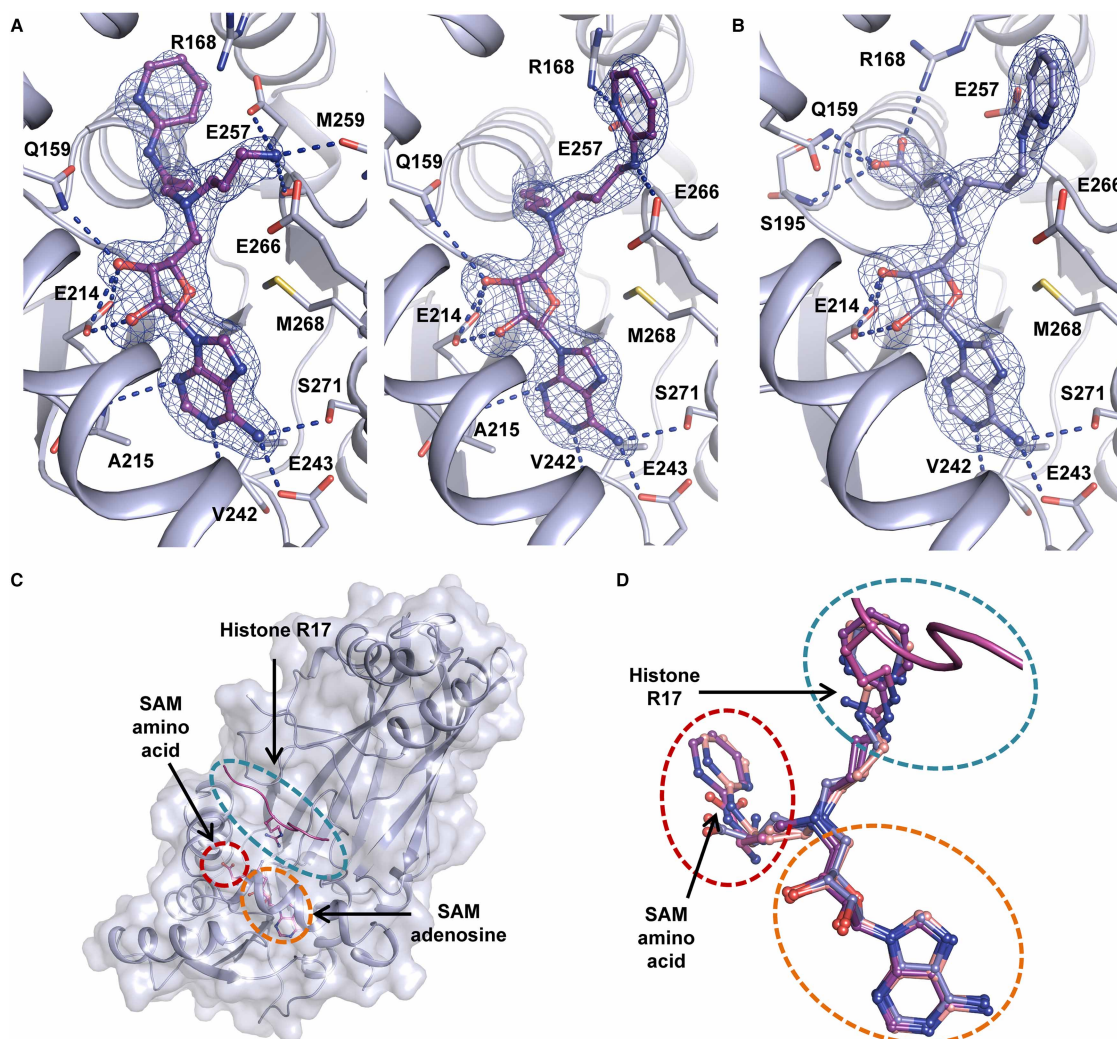
Figure 3. Crystal structures of inhibitors 9 and 10 in complex with CARM1.

(**A**) 2mF$_o$-DF$_c$ electron density maps contoured at σ = 1 for two monomers within the asymmetric unit of the CARM1·**9** complex structure. Polar contacts as computed by PyMol are indicated by blue dashed lines and residues involved in SAM and substrate arginine binding are shown in stick representation and are labelled; (**B**) 2mF$_o$-DF$_c$ electron density map of inhibitor **10** contoured at σ = 1. Polar contacts and relevant residues are shown as for (**A**). All monomers within the asymmetric unit of the CARM1·**10** structure have similar electron density for **10** corresponding to the same ligand conformation as depicted in (**B**). (**C**) binding pockets of adenosine (orange dashes) and SAM amino acid (red dashes), and substrate binding channel (teal dashes) generated using a CARM1·H3 tail peptide·sinefungin complex crystal structure (PDB code 5DX0) [48]. (**D**) Superposition of complex structures with ligands **8** (pale pink, two conformations observed are shown), **9** (purple, two conformations observed are shown) and **10** (blue, single conformation) with a structure of CARM1 in complex with histone 3 and sinefungin (magenta, PDB code 5DX0) [48].

mutation, CARM1 N265Y renders the substrate arginine-binding pocket more PRMT1-like. A modest decrease in the affinity of **8**, **9** and SAH for CARM1 N265Y compared with WT was observed while the K_d increased substantially from 1.11 to 143 μM for inhibitor **10** (Table 2; Supplementary Figure S8). These observations reinforce the notion that interactions between the aminopyridine and substrate binding channel are responsible for the preferential binding of **10** to CARM1 over PRMT1. To investigate the structural origin of this effect, CARM1 N265Y was co-crystallised with **10**. As hypothesised the resulting structure revealed a conformational change in Glu-266, in which the glutamate adopts a conformation whereby the plane of the carboxylate group is almost parallel to the phenol side chain of Tyr-265 (Figure 4C,D).
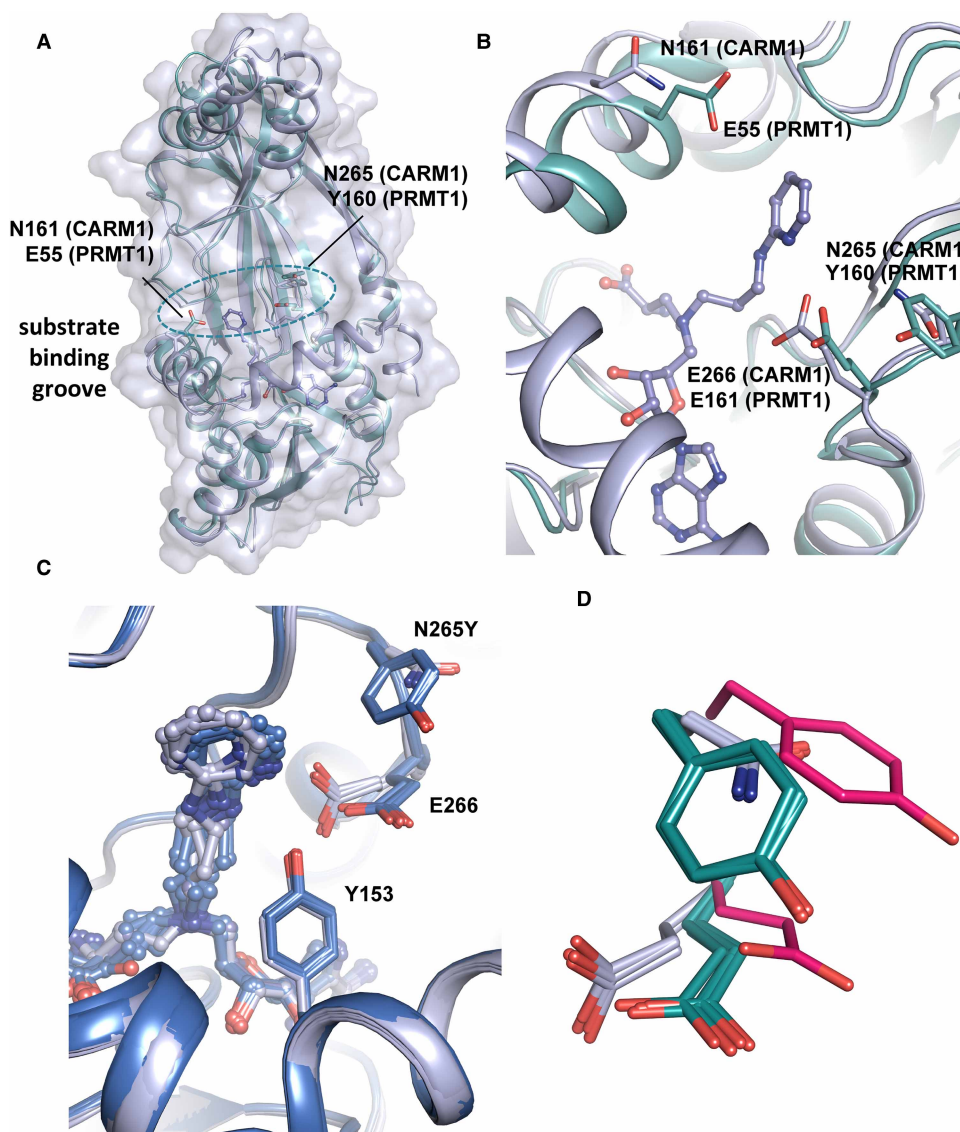
Figure 4. Structural rationale for mutagenesis and crystal structure of 10 with CARM1-N265Y.

(**A**) Superposition of CARM1·**10** complex structure (white) with a PRMT1 structure (cyan) in complex with SAH (not shown) (PDB code 1OR8 [50]). The side chains of residues targeted for mutagenesis are shown as sticks. (**B**) Zoomed-in view of position of amino acid sequence differences between PRMT1 and CARM1 investigated. (**C**) Superposition of CARM1·**10** complex structures with (blue) and without (white) the N265Y mutation. Every monomer within the asymmetric unit has been superposed. (**D**) Superposition of all CARM1(WT) monomer structures (white), all CARM1-N265Y monomers (teal) and PRMT1 (PDB code 1OR8, pink [50]).

Discussion

In this study, the binding of a novel series of non-peptidic bisubstrate inhibitors against both PRMT1 and CARM1 has been characterised. Unexpectedly, the length of a methylene linker between the guanidinium and azo adenosylmethionine moieties that comprise a subset of these inhibitors was not a determining factor for PRMT1 and CARM1 affinity, nor the position of the guanidinium group within the active site of CARM1. On testing an analogous series of amino acid-guanidine inhibitors, we previously observed a significant reduction in affinity for CARM1 on increasing the alkyl linker length from 3 to 5 methylene units [34]. In contrast with previous results, a weak interaction of the 5C amino acid-guanidine **7** with both PRMT1 and CARM1 was detected, exhibiting IC$_{50}$ and K_{d} values of 20–40 μM. Binding of **7** to CARM1 is also evidenced by the clear

Table 2 K_d values for isosteric inhibitors and 5C amino acid 7 against CARM1 single site PRMT1-mimicking mutants N161E and N265Y measured using ITC

| CARM1 | $K_d \pm$ standard error from curve fitting (µM) | | | | |
	7	8	9	10	SAH
WT	38.1 ± 9.61	2.30 ± 0.162	1.14 ± 0.411	1.11 ± 0.132	0.774 ± 0.111
N161E	8.18 ± 0.482	1.11 ± 0.201	0.354 ± 0.034	0.181 ± 0.017	0.133 ± 0.022
N265Y	-[1]	5.18 ± 1.86	3.26 ± 0.458	143 ± 75.9[2]	1.49 ± 0.063

[1]Not tested.
[2]Stoichiometry fixed to 1. Low sigmoidicity makes this value unreliable.

electron density in a co-crystal structure (Figure 2D). The apparent difference between these results and those previously reported regarding inhibitor **7** may be a result of the different CARM1 constructs used. In order to be able to compare trends from the measured dissociation constants by ITC and IC_{50} values we focused on the catalytic core of CARM1 [34]. It has been reported that indole and pyrazole CARM1 inhibitors displayed different relative potency when tested using an activity assay with GST-tagged full-length protein and ITC with the catalytic core [41]. It is possible that the presence of the GST-tag or additional regions of CARM1 outside of the catalytic core influence inhibitor binding. Elucidating a structure of full-length CARM1 in complex with inhibitors or its substrates, and determining the precise role of the domains flanking the catalytic core, will aid the design of CARM1 inhibitors. The bisubstrate nature of the inhibitors described herein necessitates care in interpretation of IC_{50} data. In the absence of detailed kinetic analysis (allowing conversion of IC_{50} values to K_is) an interpretation of selectivity of an inhibitor between different enzymes based on IC_{50} data [49] has to be treated with caution. Since such analysis is beyond the scope of the present study, K_d measurements (which do not suffer this complication) were obtained to enable direct comparison of the affinity of the inhibitor series for PRMT1 *versus* CARM1.

While these experiments were being conducted, binding studies on a related inhibitor series were reported. [28,33] Comparing the trends of reported IC_{50} values suggests that the optimal number of atoms between the 4′ ribose carbon and the guanidine group is three (equivalent to a 1 methylene linker in our inhibitors), or two atoms joined by a double bond. The differing assay conditions and inhibitor structures mean that these values cannot be directly compared with ours. Nonetheless, the high potency achieved with these shorter linker lengths, in combination with the inhibition and crystallographic data reported herein (Figure 2), suggest that the 3 to 5 methylene alkylguanidines in our inhibitors could be shortened to a methylguanidine group to better align the inhibitor guanidine for interaction with CARM1's active site glutamates, thus improving binding.

Both, inhibitors **9** and **10** displayed preferential binding for CARM1 over PRMT1. For **10**, a K_d estimate of 43.7 µM for PRMT1 (IC_{50} of 25.3 µM) was determined through a competition binding experiment as direct binding upon titrating **10** into PRMT1 was not observed, presumably because the heat change associated with ligand binding was below the limit of detection). This K_d value is broadly consistent with the IC_{50} value, and indicates that the inhibitors **9** and **10** binding more strongly to CARM1 over PRMT1 by ∼15- and ∼40-fold, respectively (as judged by ITC). This degree of selectivity provides a promising framework for the development of higher potency chemical probes for cellular assays. Interestingly, nine structures have recently been added to the PDB of CARM1 from *Mus musculus* in complex with different aromatic-containing bisubstrate inhibitors (PDB codes 5TBJ, 5TBI, 5TBH, 5LV3, 5LV2 [36] and 5ISB 5IS9, 6DVR and 6D2L [38]). Superposition of these structures with the CARM1–**9** complex structure (Supplementary Figure S9) revealed reasonably good overlap of **9**'s aminopyridine group with the aromatic groups of these inhibitors, particularly in the SAM carboxylate binding pocket (i.e. superposition with SKI-72, Supplementary Figure S9). The presence of aromatic groups in this pocket further supports our finding that **8** and **9** adopt alternate conformation in which the aromatic group may occupy either the substrate binding channel or the SAM carboxylate binding pocket (Figure 3). The observed trend towards increased potency for CARM1 by using hydrophobic guanidine isosteres will be useful in the pursuit of additional CARM1 chemical probes.

Mutagenesis studies revealed that CARM1 Asn-265 may be important for the binding of inhibitors with hydrophobic guanidine isosteres (**9** and **10**). The effect of this mutation on the position of Glu-266 in the crystal structure of CARM1 N265Y is notable. It has been suggested that the corresponding glutamate
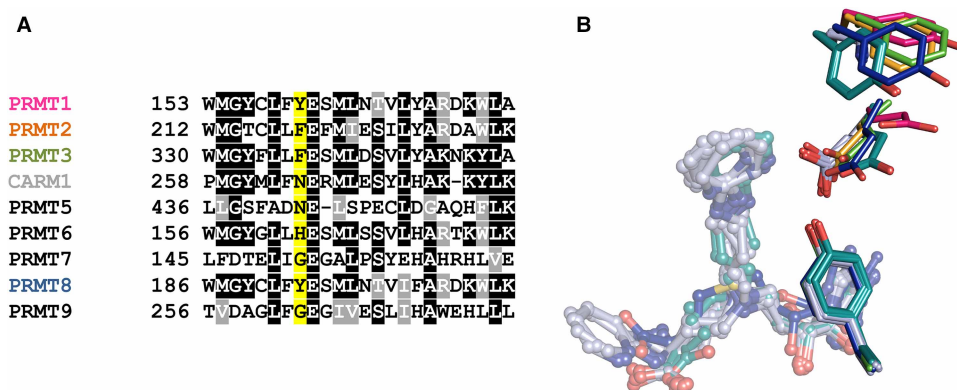
Figure 5. Sequence conservation of CARM1-N265 across other PRMTs and position of substrate arginine-interacting glutamic acid residue in PRMT structures.

(**A**) Sequence alignment of human PRMT active sites showing site of N265Y mutation generated using ClustalW and Box Shade. The site targeted for mutagenesis is highlighted in yellow. Sites that show >50% consensus are shaded (black for identical residues and grey for similar residues). Colour coding matches the structures shown in (**B**). (**B**) Superposition of PRMT1 (1OR8, hot pink [50]), PRMT2 (5JMQ, yellow), PRMT3 (1F3L, green [51]) and PRMT8 (5DST, blue [52]) with CARM1 (WT) (bound to **9**, light grey, all monomers in the asymmetric unit shown) and CARM1-N265Y (bound to **10**, teal), which all have a tyrosine or phenylalanine adjacent to the active site glutamate.

(Glu-161) in PRMT1 [50] is catalytically incompetent since it appears to be rotated away from the active site (PDB code 1OR8) [48,50]. This was attributed to likely protonation of Glu-161 due to the low pH at which the crystals formed. However, these studies reveal that substitution of CARM1 Asn-265 with a tyrosine, as present in PRMT1, results in a conformation of the glutamate side chain similar to PRMT1 in crystals grown at a pH of 7.0. This suggests that this alteration in the glutamate conformation is predominantly a result of interaction with the neighbouring tyrosine, rather than protonation of the side chain carboxylate. A sequence alignment of human PRMTs (Figure 5A) reveals that PRMTs 1, 2, 3, 6 and 8 have aromatic side chains in this position (Y, F, F, H, Y, respectively), while PRMTs 4, 5, 7 and 9 have non-aromatic side chains (N, N, G, G, respectively). A superposition of available PRMT structures with tyrosine or phenylalanine adjacent to the conserved glutamate (Figure 5B) shows that PRMT8, which has a tyrosine in this position exhibits a conformation of the neighbouring glutamate similar to that seen in the CARM1-N265Y mutant. The glutamate side chains of PRMT2 and PRMT3 (which have a phenylalanine at this position) are closer to that seen in WT CARM1. Further investigation will be required to determine the extent to which these sequence differences can be exploited for selective PRMT inhibitor development.

Crystal structures (Figure 3) show that inhibitors **8** and **9**, which feature terminal primary amines, may adopt an alternative binding conformation that positions the aminopyridine group into the subsite that normally binds the amino acid terminus of SAM. In contrast, inhibitor **10** has an amino acid terminus and adopts a single conformation that places the aminopyridine in the arginine-binding channel. This suggests that the inhibitor carboxylate group may be required to ensure the arginine mimic occupies the desired pocket. Despite conferring this apparent conformational preference, the carboxylate group does not appear to enhance the affinity of our series of inhibitors for CARM1, with **9** and **10** displaying similar K_d and IC_{50} values (Table 1). Furthermore, addition of a carboxylate group to 5C guanidine-amine **3** (i.e. inhibitor **4**) resulted in a slight decrease in potency. A terminal amino acid group (as in **7** and **10**), or appropriate isosteric replacement may therefore be beneficial for ensuring that the arginine mimicking group exclusively occupies the substrate binding channel in a single binding mode, as achieved by SAM for catalysis.

Overall, these results demonstrate effective incorporation of isosteric replacement of guanidine for a less polar 2-aminopyridine into bisubstrate PRMT inhibitors. Investigation of further isosteric replacements will be required to achieve greater rigidity, potency and cell permeability displayed by current lead compounds. Different binding for these inhibitors between CARM1 and PRMT1 prompted structural investigation which revealed differences at equivalent positions in the substrate channels for these respective enzymes (i.e. Asn-265 in CARM1 or Tyr-160 in PRMT1). Further investigation of binding and potency for bisubstrate inhibitors with

other PRMTs that feature these differences will help determine whether they can be exploited to confer selectivity to future inhibitor designs.

Competing Interests

The authors declare that there are no competing interests associated with the manuscript.

Author Contribution

E.G. carried out biophysical and biochemical characterisation of compounds, structural studies and wrote the manuscript. A.A. assisted with protein production, crystallisations and synthesised **9** and **10**, U.M. synthesised other compounds, C.D. assisted with activity assays. J.D., I.D. designed the study and its experiments and edited the manuscript.

Data Availability

Atomic co-ordinates and structure factors were deposited in the Protein Data Bank (http://wwpdb.org/) under accession IDs 6S7C, 6S7B, 6S70, 6S71, 6S74, 6S7A, 6S79 and 6S77.

Abbreviations

aDMA, asymmetric dimethylarginine; AML, acute myeloid leukemia; Bis-tris propane, 1,3-Bis[tris(hydroxymethyl) methylamino]propane; BSA, bovine serum albumin; CARM1, co-activator associated arginine methyltransferase 1; DPM, disintegrations per minute; GST, glutathione-S-transferase;; IC_{50}, inhibitor concentration giving half maximal inhibition; ITC, isothermal titration calorimetry; K_d, dissociation constant; K_i, inhibition constant; MBP, maltose binding protein; MMA, monomethyl arginine; PDB, Protein data bank; PRMT, protein arginine methyltransferase; SAH, *S*-Adenosylhomocysteine; SAM, *S*-Adenosylmethionine; sDMA, symmetric dimethylarginine; TEV, tobacco etch virus; WT, wild-type.

References

1 Wang, H., Huang, Z.-Q., Xia, L., Feng, Q., Erdjument-Bromage, H., Strahl, B.D. et al. (2001) Methylation of histone H4 at arginine 3 facilitating transcriptional activation by nuclear hormone receptor. *Science* **293**, 853 https://doi.org/10.1126/science.1060781

2 Di Lorenzo, A. and Bedford, M.T. (2011) Histone arginine methylation. *FEBS Lett.* **585**, 2024–2031 https://doi.org/10.1016/j.febslet.2010.11.010

3 Strahl, B.D., Briggs, S.D., Brame, C.J., Caldwell, J.A., Koh, S.S., Ma, H. et al. (2001) Methylation of histone H4 at arginine 3 occurs in vivo and is mediated by the nuclear receptor coactivator PRMT1. *Curr. Biol.* **11**, 996–1000 https://doi.org/10.1016/S0960-9822(01)00294-9

4 Rajakumara, E., Wang, Z., Ma, H., Hu, L., Chen, H., Lin, Y. et al. (2011) PHD finger recognition of unmodified histone H3R2 links UHRF1 to regulation of euchromatic gene expression. *Mol. Cell* **43**, 275–284 https://doi.org/10.1016/j.molcel.2011.07.006

5 Yang, Y., McBride, K.M., Hensley, S., Lu, Y., Chedin, F. and Bedford, M.T. (2014) Arginine methylation facilitates the recruitment of TOP3B to chromatin to prevent R loop accumulation. *Mol. Cell* **53**, 484–497 https://doi.org/10.1016/j.molcel.2014.01.011

6 Rezai-Zadeh, N., Zhang, X., Namour, F., Fejer, G., Wen, Y.-D., Yao, Y.-L. et al. (2003) Targeted recruitment of a histone H4-specific methyltransferase by the transcription factor YY1. *Genes Dev.* **17**, 1019–1029 https://doi.org/10.1101/gad.1068003

7 Chen, D., Ma, H., Hong, H., Koh, S.S., Huang, S.M., Schurter, B.T. et al. (1999) Regulation of transcription by a protein methyltransferase. *Science* **284**, 2174–2177 https://doi.org/10.1126/science.284.5423.2174

8 Jahan, S. and Davie, J.R. (2015) Protein arginine methyltransferases (PRMTs): role in chromatin organization. *Adv. Biol. Regul.* **57**, 173–184 https://doi.org/10.1016/j.jbior.2014.09.003

9 Cheng, D., Côté, J., Shaaban, S. and Bedford, M.T. (2007) The arginine methyltransferase CARM1 regulates the coupling of transcription and mRNA processing. *Mol. Cell* **25**, 71–83 https://doi.org/10.1016/j.molcel.2006.11.019

10 Zhang, L., Tran, N.-T., Su, H., Wang, R., Lu, Y., Tang, H. et al. (2015) Cross-talk between PRMT1-mediated methylation and ubiquitylation on RBM15 controls RNA splicing. *eLife* **4**, e07938 https://doi.org/10.7554/eLife.07938

11 Vadnais, C., Chen, R., Fraszczak, J., Yu, Z., Boulais, J., Pinder, J. et al. (2018) GFI1 facilitates efficient DNA repair by regulating PRMT1 dependent methylation of MRE11 and 53BP1. *Nat. Commun.* **9**, 1418 https://doi.org/10.1038/s41467-018-03817-5

12 Lee, Y.-H., Bedford, M.T. and Stallcup, M.R. (2011) Regulated recruitment of tumor suppressor BRCA1 to the p21 gene by coactivator methylation. *Genes Dev.* **25**, 176–188 https://doi.org/10.1101/gad.1975811

13 Lee, Y.-H. and Stallcup, M.R. (2011) Roles of protein arginine methylation in DNA damage signaling pathways. *Cell Cycle* **10**, 1343–1344 https://doi.org/10.4161/cc.10.9.15379

14 Morales, Y., Cáceres, T., May, K. and Hevel, J.M. (2016) Biochemistry and regulation of the protein arginine methyltransferases (PRMTs). *Arch. Biochem. Biophys.* **590**, 138–152 https://doi.org/10.1016/j.abb.2015.11.030

15 Yang, Y. and Bedford, M.T. (2013) Protein arginine methyltransferases and cancer. *Nat. Rev. Cancer* **13**, 37–50 https://doi.org/10.1038/nrc3409

16 Blanc, R.S. and Richard, S. (2017) Arginine methylation: the coming of age. *Mol. Cell* **65**, 8–24 https://doi.org/10.1016/j.molcel.2016.11.003

17 Guccione, E. and Richard, S. (2019) The regulation, functions and clinical relevance of arginine methylation. *Nat. Rev. Mol. Cell Biol.* **20**, 642–657 https://doi.org/10.1038/s41580-019-0155-x

18 Cheng, H., Qin, Y., Fan, H., Su, P., Zhang, X., Zhang, H. et al. (2013) Overexpression of CARM1 in breast cancer is correlated with poorly characterized clinicopathologic parameters and molecular subtypes. *Diagn. Pathol.* **8**, 129 https://doi.org/10.1186/1746-1596-8-129

19 Hong, H., Kao, C., Jeng, M.H., Eble, J.N., Koch, M.O., Gardner, T.A. et al. (2004) Aberrant expression of CARM1, a transcriptional coactivator of androgen receptor, in the development of prostate carcinoma and androgen-independent status. *Cancer* **101**, 83–89 https://doi.org/10.1002/cncr.20327

20 Elakoum, R., Gauchotte, G., Oussalah, A., Wissler, M.P., Clement-Duchene, C., Vignaud, J.M. et al. (2014) CARM1 and PRMT1 are dysregulated in lung cancer without hierarchical features. *Biochimie* **97**, 210–218 https://doi.org/10.1016/j.biochi.2013.10.021

21 Osada, S., Suzuki, S., Yoshimi, C., Matsumoto, M., Shirai, T., Takahashi, S. et al. (2013) Elevated expression of coactivator-associated arginine methyltransferase 1 is associated with early hepatocarcinogenesis. *Oncol. Rep.* **30**, 1669–1674 https://doi.org/10.3892/or.2013.2651

22 Ou, C.Y., LaBonte, M.J., Manegold, P.C., So, A.Y., Ianculescu, I., Gerke, D.S. et al. (2011) A coactivator role of CARM1 in the dysregulation of beta-catenin activity in colorectal cancer cell growth and gene expression. *Mol. Cancer Res.* **9**, 660–670 https://doi.org/10.1158/1541-7786.MCR-10-0223

23 Drew, A.E., Moradei, O., Jacques, S.L., Rioux, N., Boriack-Sjodin, A.P., Allain, C. et al. (2017) Identification of a CARM1 inhibitor with potent in vitro and in vivo activity in preclinical models of multiple myeloma. *Sci. Rep.* **7**, 17993 https://doi.org/10.1038/s41598-017-18446-z

24 Greenblatt, S.M., Man, N., Hamard, P.-J., Asai, T., Karl, D., Martinez, C. et al. (2018) CARM1 is essential for myeloid leukemogenesis but dispensable for normal hematopoiesis. *Cancer Cell* **33**, 1111–1127.e1115 https://doi.org/10.1016/j.ccell.2018.05.007

25 Knuhtsen, A., Legrand, B., Van der Poorten, O., Amblard, M., Martinez, J., Ballet, S. et al. (2016) Conformationally constrained peptidomimetics as inhibitors of the protein arginine methyl transferases. *Chem. Eur. J.* **22**, 14022–14028 https://doi.org/10.1002/chem.201602518

26 Lakowski, T.M., 't Hart, P., Ahern, C.A., Martin, N.I. and Frankel, A. (2010) Nη-substituted arginyl peptide inhibitors of protein arginine N-methyltransferases. *ACS Chem. Biol.* **5**, 1053–1063 https://doi.org/10.1021/cb100161u

27 't Hart, P., Lakowski, T.M., Thomas, D., Frankel, A. and Martin, N.I. (2011) Peptidic partial bisubstrates as inhibitors of the protein arginine N-methyltransferases. *ChemBioChem* **12**, 1427–1432 https://doi.org/10.1002/cbic.201100074

28 van Haren, M.J., Marechal, N., Troffer-Charlier, N., Cianciulli, A., Sbardella, G., Cavarelli, J. et al. (2017) Transition state mimics are valuable mechanistic probes for structural studies with the arginine methyltransferase CARM1. *Proc. Natl Acad. Sci. U.S.A.* **114**, 3625–3630 https://doi.org/10.1073/pnas.1618401114

29 Dillon, M.B.C., Bachovchin, D.A., Brown, S.J., Finn, M.G., Rosen, H., Cravatt, B.F. et al. (2012) Novel inhibitors for PRMT1 discovered by high-throughput screening using activity-based fluorescence polarization. *ACS Chem. Biol.* **7**, 1198–1204 https://doi.org/10.1021/cb300024c

30 Wang, J., Chen, L., Sinha, S.H., Liang, Z., Chai, H., Muniyan, S. et al. (2012) Pharmacophore-based virtual screening and biological evaluation of small molecule inhibitors for protein arginine methylation. *J. Med. Chem.* **55**, 7978–7987 https://doi.org/10.1021/jm300521m

31 Spannhoff, A., Heinke, R., Bauer, I., Trojer, P., Metzger, E., Gust, R. et al. (2007) Target-based approach to inhibitors of histone arginine methyltransferases. *J. Med. Chem.* **50**, 2319–2325 https://doi.org/10.1021/jm061250e

32 Nakayama, K., Szewczyk, M.M., Dela Sena, C., Wu, H., Dong, A., Zeng, H. et al. (2018) TP-064, a potent and selective small molecule inhibitor of PRMT4 for multiple myeloma. *Oncotarget* **9**, 18480–18493 https://doi.org/10.18632/oncotarget.24883

33 van Haren, M., van Ufford, L.Q., Moret, E.E. and Martin, N.I. (2015) Synthesis and evaluation of protein arginine N-methyltransferase inhibitors designed to simultaneously occupy both substrate binding sites. *Org. Biomol. Chem.* **13**, 549–560 https://doi.org/10.1039/C4OB01734J

34 Dowden, J., Pike, R.A., Parry, R.V., Hong, W., Muhsen, U.A. and Ward, S.G. (2011) Small molecule inhibitors that discriminate between protein arginine N-methyltransferases PRMT1 and CARM1. *Org. Biomol. Chem.* **9**, 7814–7821 https://doi.org/10.1039/c1ob06100c

35 Yang, H., Ouyang, Y., Ma, H., Cong, H., Zhuang, C., Lok, W.T. et al. (2017) Design and synthesis of novel PRMT1 inhibitors and investigation of their binding preferences using molecular modelling. *Bioorg. Med. Chem. Lett.* **27**, 4635–4642 https://doi.org/10.1016/j.bmcl.2017.09.016

36 Halby, L., Marechal, N., Pechalrieu, D., Cura, V., Franchini, D.-M., Faux, C. et al. (2018) Hijacking DNA methyltransferase transition state analogues to produce chemical scaffolds for PRMT inhibitors. *Philos. Trans. R. Soc. B* **373**, 20170072 https://doi.org/10.1098/rstb.2017.0072

37 Fuhrmann, J., Clancy, K.W. and Thompson, P.R. (2015) Chemical biology of protein arginine modifications in epigenetic regulation. *Chem. Rev.* **115**, 5413–5461 https://doi.org/10.1021/acs.chemrev.5b00003

38 Cai, X.C., Zhang, T., Kim, E.J., Jiang, M., Wang, K., Wang, J. et al. (2019) A chemical probe of CARM1 alters epigenetic plasticity against breast cancer cell invasion. *eLife* **8**, e47110 https://doi.org/10.7554/eLife.47110

39 Moon, A.F., Mueller, G.A., Zhong, X. and Pedersen, L.C. (2010) A synergistic approach to protein crystallization: combination of a fixed-arm carrier with surface entropy reduction. *Protein Sci.* **19**, 901–913 https://doi.org/10.1002/pro.368

40 McCoy, A.J., Grosse-Kunstleve, R.W., Adams, P.D., Winn, M.D., Storoni, L.C. and Read, R.J. (2007) Phaser crystallographic software. *J. Appl. Crystallogr.* **40**, 658–674 https://doi.org/10.1107/S0021889807021206

41 Sack, J.S., Thieffine, S., Bandiera, T., Fasolini, M., Duke, G.J., Jayaraman, L. et al. (2011) Structural basis for CARM1 inhibition by indole and pyrazole inhibitors. *Biochem. J.* **436**, 331 https://doi.org/10.1042/BJ20102161

42 Emsley, P., Lohkamp, B., Scott, W.G. and Cowtan, K. (2010) Features and development of Coot. *Acta Crystallogr. D* **66**, 486–501 https://doi.org/10.1107/S0907444910007493

43 Adams, P.D., Afonine, P.V., Bunkóczi, G., Chen, V.B., Davis, I.W., Echols, N. et al. (2010) PHENIX: a comprehensive Python-based system for macromolecular structure solution. *Acta Crystallogr. D* **66**, 213–221 https://doi.org/10.1107/S0907444909052925

44 Murshudov, G.N., Vagin, A.A. and Dodson, E.J. (1997) Refinement of macromolecular structures by the maximum-likelihood method. *Acta Crystallogr. D* **53**, 240–255 https://doi.org/10.1107/S0907444996012255

45 Moriarty, N.W., Grosse-Kunstleve, R.W. and Adams, P.D. (2009) Electronic ligand builder and optimization workbench (eLBOW): a tool for ligand coordinate and restraint generation. *Acta Crystallogr. D* **65**, 1074–1080 https://doi.org/10.1107/S0907444909029436

46   Brown, D.J. and Paddon-Row, M.N. (1966) The Dimroth rearrangement. Part VI. The abnormal behaviour of 5-cyano-1,2-dihydro-2-imino-1-methylpyrimidine. *J. Chem. Soc. C*, 164–166 https://doi.org/10.1039/j39660000164

47   Peral, F. and Gallego, E. (1994) Self-association of pyridine and some of its derivatives in aqueous solution: influence of alkyl substituents. *J. Mol. Struct.* **326**, 59–68 https://doi.org/10.1016/0022-2860(94)08330-4

48   Boriack-Sjodin, P.A., Jin, L., Jacques, S.L., Drew, A., Sneeringer, C., Scott, M.P. et al. (2016) Structural insights into ternary complex formation of human CARM1 with various substrates. *ACS Chem. Biol.* **11**, 763–771 https://doi.org/10.1021/acschembio.5b00773

49   Jingsong, Y., Robert, A.C. and Zhihong, L. (2009) Defining balanced conditions for inhibitor screening assays that target bisubstrate enzymes. *J. Biomol. Screen.* **14**, 111–120 https://doi.org/10.1177/1087057108328763

50   Zhang, X. and Cheng, X. (2003) Structure of the predominant protein arginine methyltransferase PRMT1 and analysis of its binding to substrate peptides. *Structure* **11**, 509–520 https://doi.org/10.1016/S0969-2126(03)00071-6

51   Zhang, X., Zhou, L. and Cheng, X. (2000) Crystal structure of the conserved core of protein arginine methyltransferase PRMT3. *EMBO J.* **19**, 3509–3519 https://doi.org/10.1093/emboj/19.14.3509

52   Toma-Fukai, S., Kim, J.D., Park, K.E., Kuwabara, N., Shimizu, N., Krayukhina, E. et al. (2016) Novel helical assembly in arginine methyltransferase 8. *J. Mol. Biol.* **428**, 1197–1208 https://doi.org/10.1016/j.jmb.2016.02.007

Supplementary experimental data for compounds 5, 6, 8, 9 and 10

5 - 1-(4-((((2*R*,3*S*,4*R*,5*R*)-5-(6-amino-9*H*-purin-9-yl)-3,4-dihydroxytetrahydro furan-2-yl)methyl)(3-aminopropyl)amino)butyl)guanidine hydrochloride: $[\alpha]^{23}_D$ 17.66; ν_{max}/cm^{-1} 3317, 3167, 1683, 1051; ^{1}H NMR (400 MHz, D$_2$O) δ_H 8.46 (s, 1H, Ad-*H*), 8.44 (s, 1H, Ad-*H*), 6.14 (d, *J*=4.0 Hz, 1H, 1'-*H*), 4.79 (m, 1H, 2'-*H*), 4.44-4.52 (m, 2H, 3'-*H* and 4'-*H*), 3.73-3.79 (1H, m, 5'-C*H*aH$_b$), 3.67 (dd, *J*=14.0, 1.6, 1H, 5'-CH$_a$*H*$_b$), 3.35 (t, *J*=8.1, 2H, C*H*$_2$), 3.29 (t, *J*=8.3, 2H, C*H*$_2$), 3.02-3.06 (m, 4H, C*H*$_2$ and C*H*$_2$), 2.08-2.15 (m, 2H, C*H*$_2$), 1.71-1.73 (m, 2H, C*H*$_2$), 1.52-1.54 (m, 2H, C*H*$_2$); ^{13}C NMR (100 MHz, D$_2$O) δ_C 156.6, 150.1, 148.1, 144.7, 143.4, 119.1, 89.9, 78.0, 73.1, 71.5, 54.7, 53.0, 50.5, 40.4, 36.6, 24.9, 21.5, 20.2. HRMS (ESI+) m/z: (M+H $^+$) calcd C$_{18}$H$_{33}$N$_{10}$O$_3$$^+$ 437.2737, found 437.2731.

6 - 3-((4-((amino(iminio)methyl)amino)butyl)(((2*R*,3*S*,4*R*,5*R*)-5-(6-amino-9*H*-purin-9-yl)-3,4-dihydroxytetrahydrofuran-2-yl)methyl)amino)propan-1-aminium chloride $[\alpha]^{23}_D$ +23.55 (c 1.0 in H$_2$O); ν_{max}/cm^{-1} 3363, 1647, 1436, 1120. ^{1}H NMR (400 MHz, D$_2$O) δ_H: 8.42 (s, 1H, Ad-*H*), 8.40 (s, 1H, Ad-*H*), 6.12 (d, *J*=4.0 Hz, 1H, 1'-*H*), 4.80-4.51 (m, 1H, 2'-*H*), 4.43-4.51 (m, 2H, 3'-*H* and 4'-*H*), 3.72-3.78 (1H, m, 5'-C*H*aH$_b$), 3.66 (d, *J*=14.0 Hz, 1H, 5'-CH$_a$*H*$_b$), 3.32 (t, *J*=7.8, 2H, C*H*$_2$), 3.24 (t, *J*=7.9, 2H, C*H*$_2$), 3.00-3.04 (m, 4H, C*H*$_2$ and C*H*$_2$), 2.08-2.15 (m, 2H, C*H*$_2$), 1.65-1.75 (m, 2H, C*H*$_2$), 1.40-1.45 (m, 2H, C*H*$_2$), 1.24-1.28 (m, 2H, C*H*$_2$); ^{13}C NMR (100 MHz, D$_2$O) δ_C: 156.6, 150.7, 148.2, 145.7, 143.1 , 119.2, 89.9, 78.0, 73.0, 71.6, 54.8, 53.3, 50.5, 40.8, 36.5, 27.3, 23.6, 22.8, 21.5. HRMS (ESI+) m/z: (M+H$^+$) calcd C$_{19}$H$_{35}$N$_{10}$O$_3$$^+$ 451.2894, found 451.2901.

8 - 3-((((2R,3S,4R,5R)-5-(6-amino-9H-purin-9-yl)-3,4-dihydroxytetrahydrofuran-2-yl)methyl)(3-(pyrimidin-2-ylamino)propyl)amino)propan-1-aminium chloride: $[\alpha]^{23}_D$ +23.55 (c 1.0 in H$_2$O); ν_{max}/cm^{-1} 3084, 1644, 1052; ^{1}H NMR (400 MHz, D$_2$O) δ_H: 8.09 (s, 1H, Ad-H), 8.01 (s, 1H, Ad-H), 7.87 (d, *J*= 4.9, 2H, Ar-H), 6.31 (app. t, *J*= 4.9, 1H, Ar-H), 5.85 (d, *J*= 4.8, 1H, 1'-H), 4.66 (app. t, *J* = 4.8, 1H, 2'-H), 4.22-4.23 (m, 1H, 3'-H), 4.15 (app. t, *J*= 5.3, 1H, 4'-H), 3.01-3.06 (m, 1H, C*H*$_a$H$_b$), 2.93-2.98 (m, 1H, CH$_a$*H*$_b$), 2.95 (t, *J*= 7.3, 2H, CH$_2$), 2.81-2.87 (1H, m, 1H, 5'-C*H*$_a$H$_b$), 2.73 (d, *J*=14.4, 1H, 5'-CH$_a$*H*$_b$), 2.61-2.67 (m, 2H, CH$_2$), 2.50-2.56 (m, 2H, CH$_2$), 1.72-1.79 (m, 2H, CH$_2$), 1.61-1.66 (m, 1H, C*H*$_a$H$_b$), 1.52-1.58 (m, 1H, CH$_a$*H*$_b$); ^{13}C NMR (100 MHz, D$_2$O) δ_C: 160.4, 157.7, 155.1, 152.5, 148.4, 139.8, 118.6, 109.9, 87.9, 81.4, 72.9, 72.0, 55.4, 51.7, 51.5, 39.4, 38.5, 24.4, 23.8; HRMS (ESI+) m/z: (M+H$^+$) calcd C$_{20}$H$_{31}$N$_{10}$O$_3$$^+$ 459.2581, found 459.2575.

9 - 3-((((2*R*,3*S*,4*R*,5*R*)-5-(6-amino-9*H*-purin-9-yl)-3,4-dihydroxytetrahydrofuran-2-yl)methyl)(3-(pyridin-2-ylamino)propyl)amino)propan-1-aminium chloride: $[\alpha]^{23}_D$ +7.40 (c 1.0 in H$_2$O); ν_{max}/cm^{-1} 3475, 3009, 1465, 1016; ^{1}H NMR (400 MHz, D$_2$O) δ_H: 8.40 (s, 1H, Ar-*H*), 7.71-7.76 (m, 1H, Ar-*H*), 7.61 (d, *J*=6.5, 1H, Ar-H), 6.83-6.86 (m, 1H, Ar-*H*), 6.75 (app t, *J*=6.5, 1H, Ar-H), 6.05 (d, *J*=3.6, 1H, 1'-*H*), 4.61 (app t, *J*= 3.6, 1H, 2'-*H*), 4.43-4.44 (m, 2H, CH and C*H*aHb), 3.80-3.82 (m, 1H, CH), 3.68 (d *J*=14.3, 1H, CH$_a$*H*$_b$), 3.63 (1H, td, *J*=6.1, 2.6, CH) 3.35-3.42 (m, 4H, and 2xC*H*$_2$), 3.00-3.12 (m, 3H, C*H*$_2$ and C*H*aCH$_b$), 2.00-2.13 (m, 4H, 2xC*H*$_2$); ^{13}C NMR (100 MHz, D$_2$O) δ_C: 152.3, 149.8, 147.8, 144.5, 143.8, 143.2, 134.8, 119.1, 112.7, 90.3, 77.5, 73.2, 71.4, 58.9, 51.10, 51.07, 48.9, 38.6, 36.4, 21.8, 21.3; HRMS (ESI+) m/z: (M+H$^+$) calcd C$_{21}$H$_{31}$N$_9$O$_3$$^+$ 458.2623, found 458.2623.

10 (*S*)-4-((((2*R*,3*S*,4*R*,5*R*)-5-(6-amino-9*H*-purin-9-yl)-3,4-dihydroxytetrahydrofuran-2-yl)methyl)(3-(pyridin-2-ylamino)propyl)amino)-2-ammoniobutanoate, chloride salt**:** $[\alpha]^{23}_D$ +20.73 (c 1.0 in H$_2$O); ν_{max}/cm^{-1} 3441 (N-H), 3007 , 1623, 1240, 1015; ^{1}H NMR (400 MHz, D$_2$O) δ_H 8.43 (s, 1*H*, adenosine-*H*), 8.39 (s, 1H, adenosine-*H*), 7.75-7.79 (m, 1H, Pyr*H*), 7.65 (d, *J*=6.2, 1H, Pyr*H*), 6.88 (d, *J*= 8.5, 1H, Pyr*H*), 6.76-6.80 (m, 1H, Pyr*H*), 6.09 (d, *J*=3.6, 1H, 1'-*H*), 4.64-4.66 (m, 1H, 2'-*H*), 4.42-4.45 (m, 2H, C*H,* CH$_a$*H*$_b$), 4.08-4.14 (m, 1H, C*H*), 3.82-3.90 (m, 1H, C*H*), 3.72 (d, J=13.6, 1H, CH$_a$*H*$_b$), 3.29-3.63 (m, 6H, C*H*$_2$), 2.38-2.48 (m, 1H, C*H*aCH$_b$CH), 2.26-2.33 (m, 1H, CH$_a$C*H*$_b$), 2.02-2.09 (m, 2H, CH$_2$C*H*$_2$CH$_2$), ^{13}C NMR (100 MHz, D$_2$O) δ_C: 170.4, 152.2, 149.7, 147.8, 144.4, 143.8, 143.2, 134.8, 119.1, 112.7, 90.3, 78.0, 73.1, 71.4, 54.7, 51.1, 50.9, 50.8, 50.5, 38.6, 24.1, 21.9; HRMS (ESI+) *m/z*: (M+H$^+$) calcd C$_{22}$H$_{31}$N$_9$O$_5$$^+$ 502.2520, found 502.2521.

Inhibitor	[CARM1]/mg/mL	Crystallisation condition
4	1.7	0.1 M Bis-tris propane pH 7.0, 0.02 M sodium phosphate, 21 % (w/v) PEG 3350
5	1.7	0.1 M Bis-tris propane pH 7.0, 0.02 M potassium phosphate, 22 % (w/v) PEG 3350
6	1.7	0.1 M Bis-tris propane pH 7.0, 0.2 M sodium acetate, 24 % (w/v) PEG 3350
7	1.2	0.1 M Bis-tris propane pH 7.0, 0.2 M sodium acetate, 20 % (w/v) PEG 3350
8	1.0	0.1 M Bis-tris propane pH 7.0, 0.02 M sodium phosphate, 22 % (w/v) PEG 3350
9	3.0	0.1 M Bis-tris propane pH 8.5, 0.2 M sodium formate, 20 % (w/v) PEG 3350
10	3.0	0.1 M Bis-tris propane pH 8.5, 0.2 M sodium formate, 20 % (w/v) PEG 3350
10 w/CARM1 N265Y	2.4	0.1 M Bis-tris propane pH 7.0, 0.02 M sodium phosphate, 26 % (w/v) PEG 3350

Table S1. Crystallisation conditions for CARM1-inhibitor complexes.
The protein concentrations indicated are the concentrations measured prior to addition of a half-volume of 500 µM ligand solution, then mixing with the well solution, as detailed in the main text.

	4	5	6	7	8	9	10	10 (CARM1 N265Y)
PDB Code	6S7C	6S7B	6S70	6S71	6S74	6S7A	6S79	6S77
Beamline	ID30B (ESRF)[1]	I02 (DLS)[2]	ID30B (ESRF)	ID30B (ESRF)	ID30B (ESRF)	I03 (DLS)	I03 (DLS)	ID30-A1 (ESRF)
Wavelength (Å)	0.9762	0.9795	0.9762	0.9762	0.9762	0.9762	0.9762	0.9800
Resolution range	51.86 - 2.30 (2.38 - 2.30)	61.12 - 2.66 (2.75 - 2.66)	57.23 - 2.30 (2.38 - 2.30)	88.99 - 2.06 (2.14 - 2.06)	48.17 - 2.1 (2.18 - 2.1)	71.42 - 1.86 (1.93 - 1.86)	69.48 - 2.10 (2.18 - 2.10)	48.01 - 2.12 (2.20 - 2.12)
Space group	P 21 21 2	P 21 21 2	P 21 21 2	P 21 21 2	P 21 21 2	P 21 21 2	P 21 21 2	P 21 21 2
Unit cell a (Å)	74.697	75.455	74.684	74.72	75.393	74.784	75.479	74.988
b (Å)	98.629	99.367	98.677	98.63	99.029	98.624	99.196	98.718
c (Å)	207.438	208.463	207.1	206.36	207.952	207.137	208.439	207.071
Total reflections	279649 (18740)	294369 (2801)	276271 (17387)	342936 (15243)	302969 (16836)	852511 (33682)	612585 (30578)	350341 (18242)
Unique reflections	66343 (4477)	45903 (437)	66028 (4361)	91634 (4501)	80206 (4644)	129298 (6329)	92162 (4483)	87715 (4472)
Multiplicity	4.2 (4.2)	6.4 (6.4)	4.2 (4.0)	3.7 (3.4)	3.8 (3.6)	6.6 (5.3)	6.6 (6.8)	4.0 (4.1)
Completeness (%)	96.7 (98.2)	99.9 (98.0)	96.2 (95.8)	96.7 (96.5)	87.8 (90.1)	100.0 (100.0)	100.0 (99.9)	99.7 (99.8)
Mean I/sigma(I)	11.8 (2.2)	10.1 (2.8)	13.8 (2.4)	11.8 (2.1)	11.6 (2.2)	9.1 (0.8)	7.4 (0.9)	8.8 (1.2)
R-merge	0.075 (0.741)	0.210 (1.052)	0.065 (0.546)	0.058 (0.538)	0.064 (0.496)	0.095 (1.829)	0.186 (2.516)	0.096 (1.176)
R-pim	0.041 (0.412)	0.090 (0.450)	0.044 (0.295)	0.033 (0.325)	0.034 (0.269)	0.040 (0.876)	0.078 (1.040)	0.054 (0.655)
$CC_{1/2}$	0.998 (0.684)	0.994 (0.781)	0.999 (0.765)	0.999 (0.780)	0.999 (0.818)	0.998 (0.393)	0.996 (0.287)	0.998 (0.431)
Refinement								
No of reflections	66203 (6645)	45808 (4499)	65966 (6428)	91546 (9039)	80113 (8094)	129154 (12752)	92043 (9068)	87609 (8680)
R-work	0.2068 (0.3141)	0.1945 (0.3060)	0.1851 (0.2571)	0.2336 (0.3088)	0.1921 (0.2845)	0.1993 (0.3201)	0.1989 (0.3268)	0.2039 (0.3111)
R-free	0.2355 (0.3306)	0.2278 (0.3406)	0.2129 (0.2893)	0.2542 (0.3531)	0.2151 (0.3084)	0.2194 (0.3504)	0.2314 (0.3406)	0.2464 (0.3230)
<B-factors> (Å^2)								
Protein	45.09	41.05	42.47	42.01	35.46	45.96	45.82	42.68
Inhibitors	50.40	53.48	49.10	57.64	35.74	48.13	47.71	42.39
RMS bond lengths (Å)	0.016	0.016	0.020	0.012	0.018	0.015	0.032	0.013
RMS bond angles (°)	1.76	1.72	1.73	1.52	1.51	1.66	2.07	1.62

Table S2. Data collection and refinement statistics for CARM1-inhibitor crystal structures. Statistics for the highest-resolution shell are given in parentheses.

PRMT1			
Inhibitor	ΔG (kJ/mol)	ΔH ± standard error from curve fitting (kJ/mol)	-TΔS (kJ/mol)	N ±standard error from curve fitting
SAH	-35.1	-97.7 ± 1.4	62.6	0.485 ± 0.0037
4	-28.5	-67 ± 3.22	38.5	0.519 ± 0.0082
5	-30.8	-48.1 ± 1.86	17.2	0.549 ± 0.0092
6	-28.6	-41.5 ± 2.79	12.9	0.607 ±0.019
7	-25.7	-27.5 ± 1.4	1.84	N/A[1]
8	-28.5	-43.2 ± 10.5	14.7	0.322 ± 0.028
9	-27.5	-29.4 ± 1.16	39.1	0.716 ± 0.012
10	-24.9	-6.71[2]	-18.2	N/A[2]

CARM1			
Inhibitor	ΔG (kJ/mol)	ΔH ± standard error from curve fitting (kJ/mol)	-TΔS (kJ/mol)	N ±standard error from curve fitting
SAH	-34.9	-147 ± 4.62	113	0.549 ± 0.0086
4	-31.3	-103 ± 2.65	71.9	0.481 ± 0.0062
5	-29.4	-110 ± 2.98	80.5	0.501 ± 0.0060
6	-28.6	-79.2 ± 6.42	50.5	0.417 ± 0.012
7	-25.2	-77.7 ± 9.65	52.5	0.648 ± 0.032
8	-32.2	-124 ± 1.86	92.2	0.529 ± 0.0042
9	-34	-86.2 ± 7.42	52.3	0.529 ± 0.025
10	-34	-73.1 ± 1.92	39.1	0.536 ± 0.0079

[1] The stoichiometry was fixed to 0.5 due to a low c-value curve.
[2] Data were determined using a competition experiment, therefore the ΔH error and binding stoichiometry are not calculated.

Table S3. Thermodynamic parameters from ITC data for inhibitors 4, 5, 6, 7, 8, 9 and 10 titrations into PRMT1 and CARM1.

ΔG, ΔH, -TΔS and stoichiometry (N) determined from titrations of SAH and inhibitors **4**, **5**, **6**, **7**, **8**, **9**, and **10** into PRMT1 (top) or CARM1 (bottom). Standard errors are not calculated for ΔG and -TΔS since they are calculated indirectly using the best-fit values of K_d and ΔH.
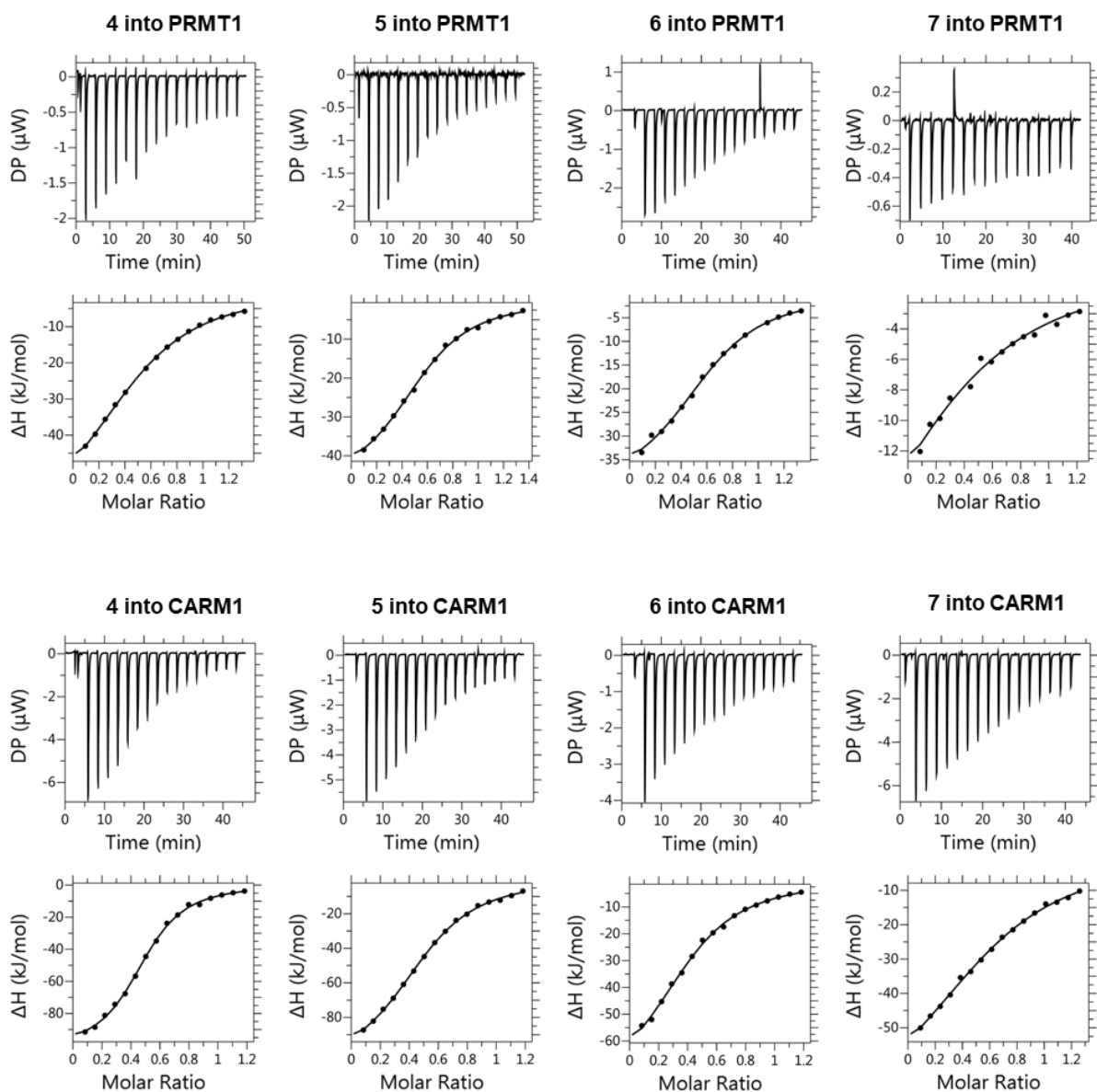
	Inhibitor	CARM1			
		ΔG (kJ/mol)	ΔH ± standard error (kJ/mol)	-TΔS (kJ/mol)	N± standard error
N161E	**SAH**	-39.3	-125 ± 1.84	86.1	0.692 ± 0.0047
	8	-34	-113 ± 3.79	79.2	0.745 ± 0.012
	9	-36.8	-86.7 ± 1.17	49.9	0.914 ± 0.005
	10	-38.5	-94.1 ± 0.971	55.6	1.02 ± 0.004
N265Y	**SAH**	-33.3	-99.1 ± 1.05	65.9	0.737 ± 0.004
	8	-30.2	-62.8 ± 8.41	32.7	0.698 ± 0.051
	9	-31.3	-61.9 ± 3.36	30.6	1.07 ± 0.035
	10	-[1]	-	-	-

[1] The low sigmoidicity of the CARM1-N265Y/**10** curve was not sufficient for reliable determination of binding parameters.

Table S4. Thermodynamic parameters from SAH and inhibitors 8, 9, and 10 titrations into CARM1 N161E and N265Y mutants.

ΔG, ΔH, -TΔS values derived from ITC data of SAH and inhibitors **8**, **9**, and **10** into CARM1 N161E and N265Y mutants are shown. Standard errors are not calculated for ΔG and -TΔS since they are calculated indirectly using the best-fit values of K_d and ΔH.

Supplementary Figures

(a)
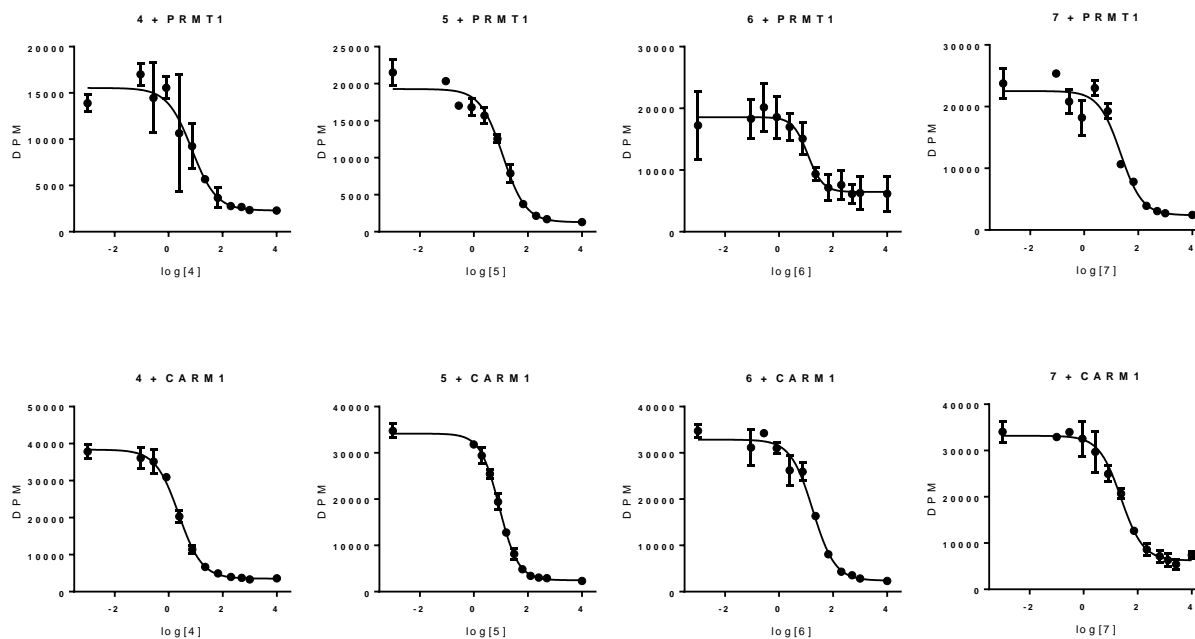
(b)
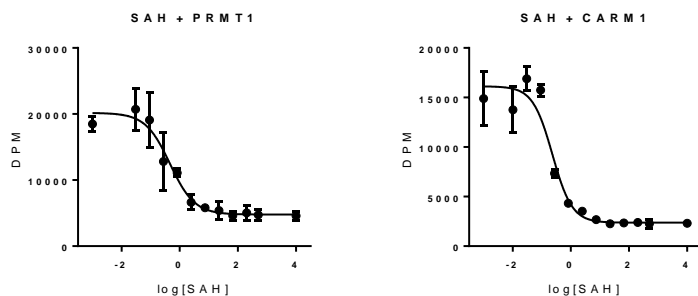
**Supplementary Figure S1. Dose-response curves for inhibitors 4, 5, 6, and 7 and SAH.**

(a) IC$_{50}$ curves for inhibitors **4**, **5** and **6** and **7** with PRMT1 and CARM1. Error bars indicate standard deviation (S.D.) at each inhibitor concentration (n=2). DPM is the un-normalised disintegrations per minute, measured by liquid scintillation counting, and is proportional to tritium incorporation into the substrate.

(b) IC$_{50}$ curves for SAH with PRMT1 and CARM1. Error bars indicate S.D. at each inhibitor concentration (n=2). DPM is the un-normalised disintegrations per minute, measured by liquid scintillation counting, and is proportional to tritium incorporation into the substrate.

Supplementary Figure S2. ITC thermograms (upper panels) and integrated heat plots (lower panels) for inhibitors 4, 5, 6 and 7.
The inhibitor and PRMT used for each titration are given above the relevant graphs. CARM1 and PRMT1 titrations were conducted at 25°C with PRMT concentrations in the range of 42 – 121 μM and inhibitor concentrations in the range of 230 – 736 μM.
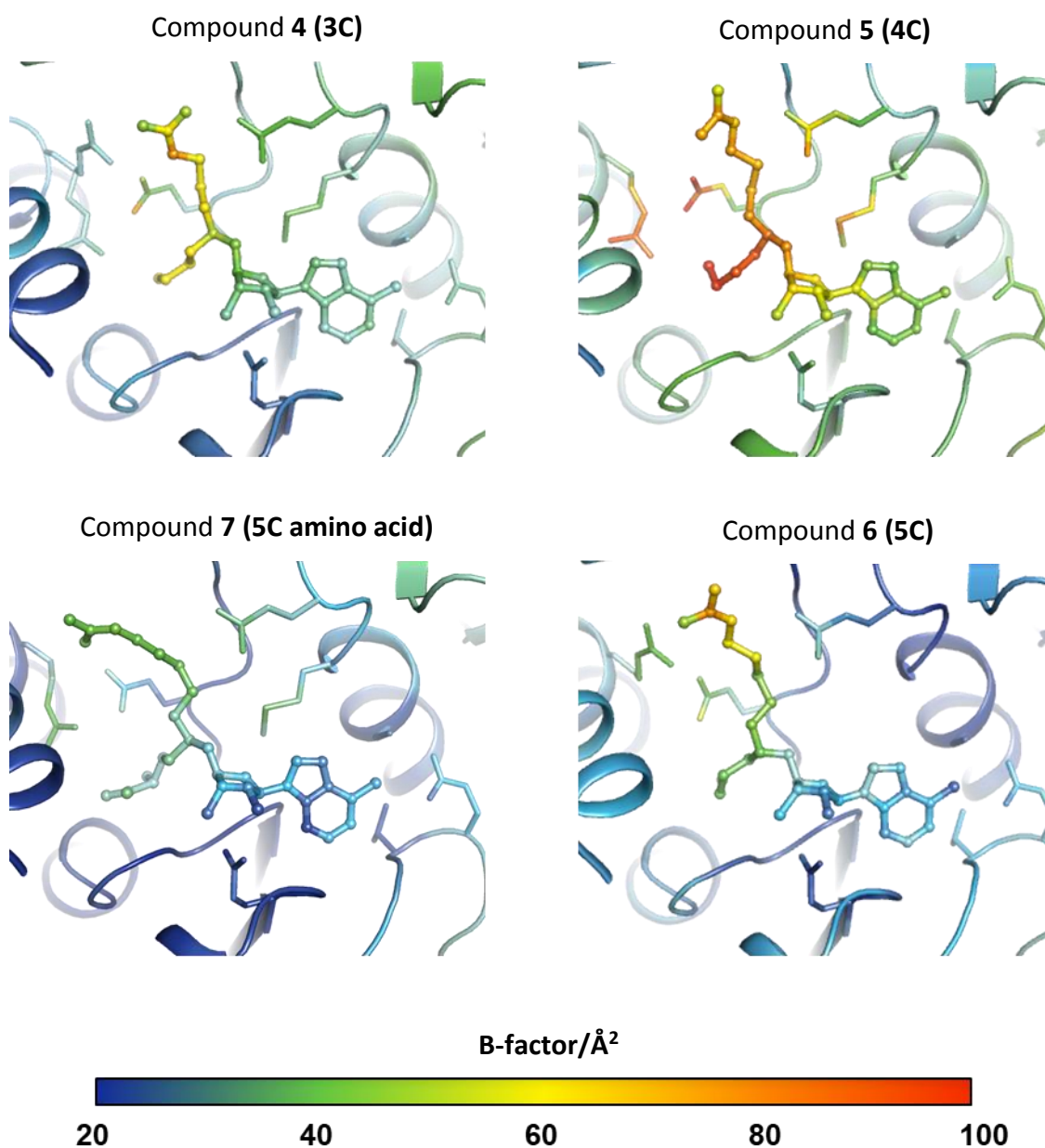
Supplementary Figure S3. Graphical representation of B-factors in respective inhibitor 4, 5, 6 and 7 – CARM1 complex crystal structures.

The structures in cartoon representation with the inhibitors shown in ball-and-stick are coloured according to B-factor values as shown in the spectrum bar below ranging from dark blue (20 Å^2) to red (100 Å^2).
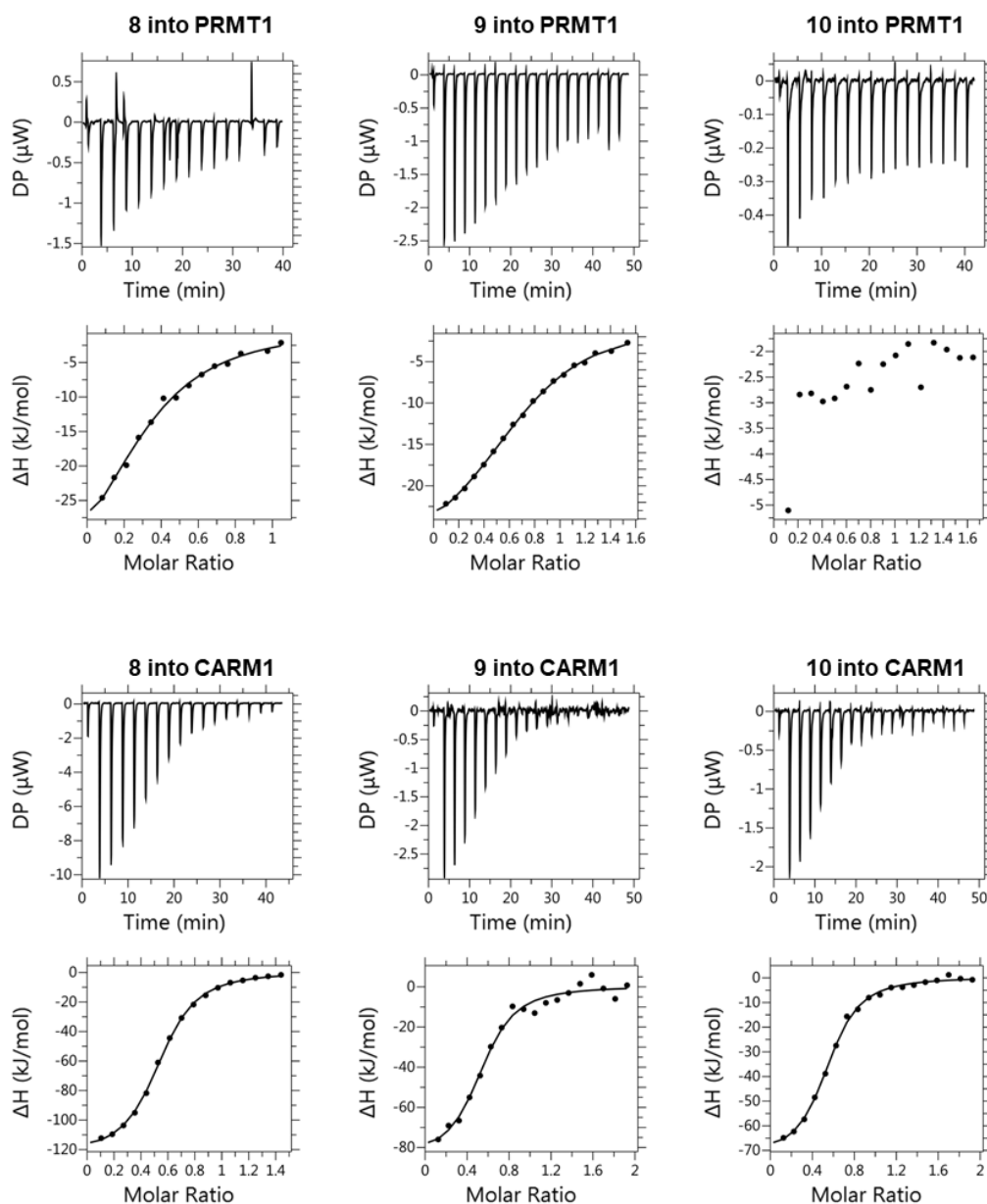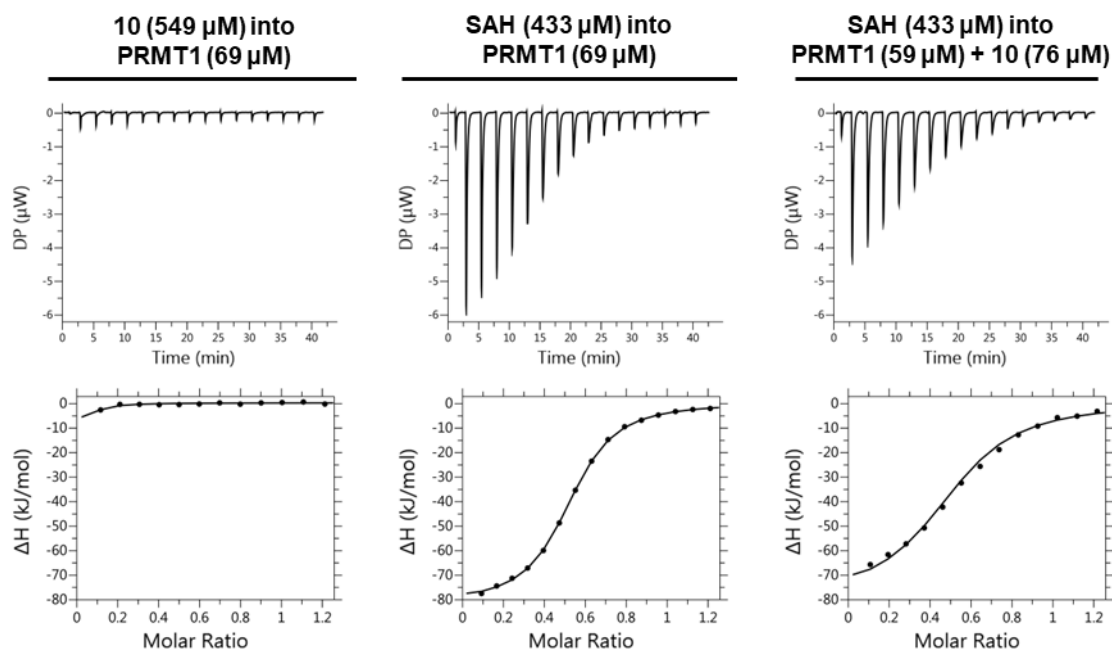
Supplementary Figure S4. ITC thermograms (upper panels) and integrated heat plots (lower panels) for inhibitors 8, 9 and 10.
The inhibitor and PRMT used for each titration are given above the relevant graphs. CARM1 and PRMT1 titrations were conducted at 25°C with PRMT concentrations in the range of 21 – 80 μM and inhibitor concentrations in the range of 210 – 600 μM in order to optimise sigmoidicity.
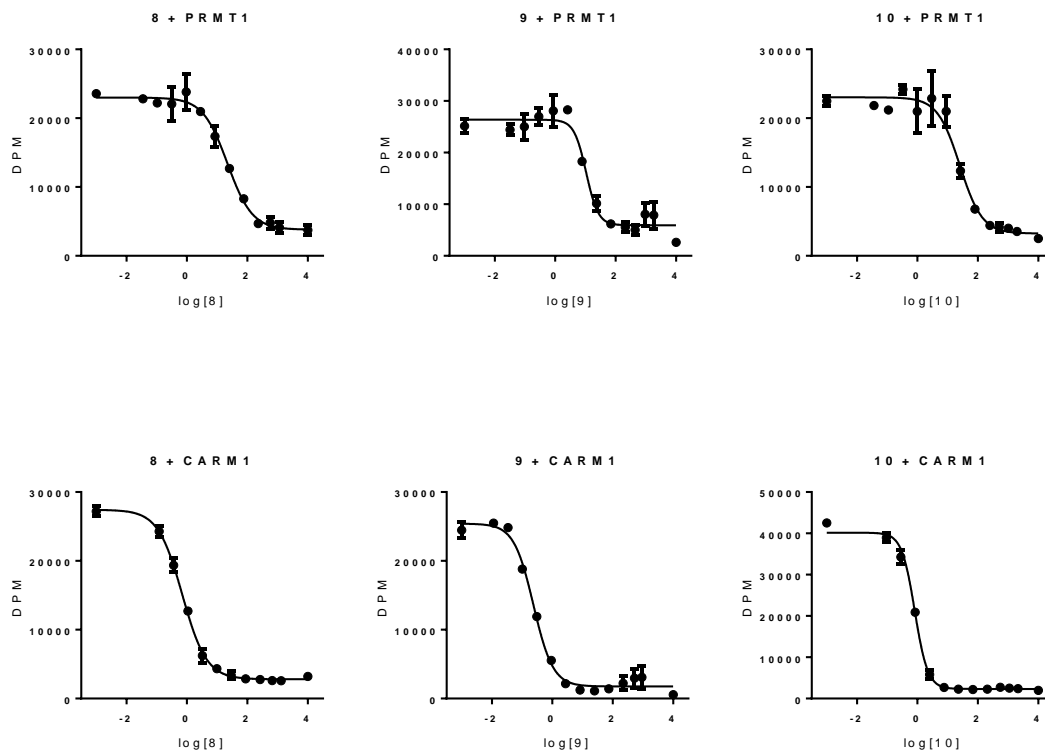
Supplementary Figure S5. Dose-response curves for inhibitors 8, 9 and 10.

IC_{50} curves for inhibitors **8**, **9** and **10** with PRMT1 and CARM1. Error bars indicate the S.D. (n=2) at each inhibitor concentration. DPM is the un-normalised disintegrations per minute, measured by liquid scintillation counting, and is proportional to tritium incorporation into the substrate.

Supplementary Figure S6. ITC experiments with PRMT1 and inhibitor 10 or SAH.
ITC thermograms (upper panels) and integrated heat plots (lower panels) for titrations of SAH into PRMT in the presence and absence of inhibitor **10** (i.e. competition ITC experiment) are shown with the respective titrant(s) indicated above the thermograms.
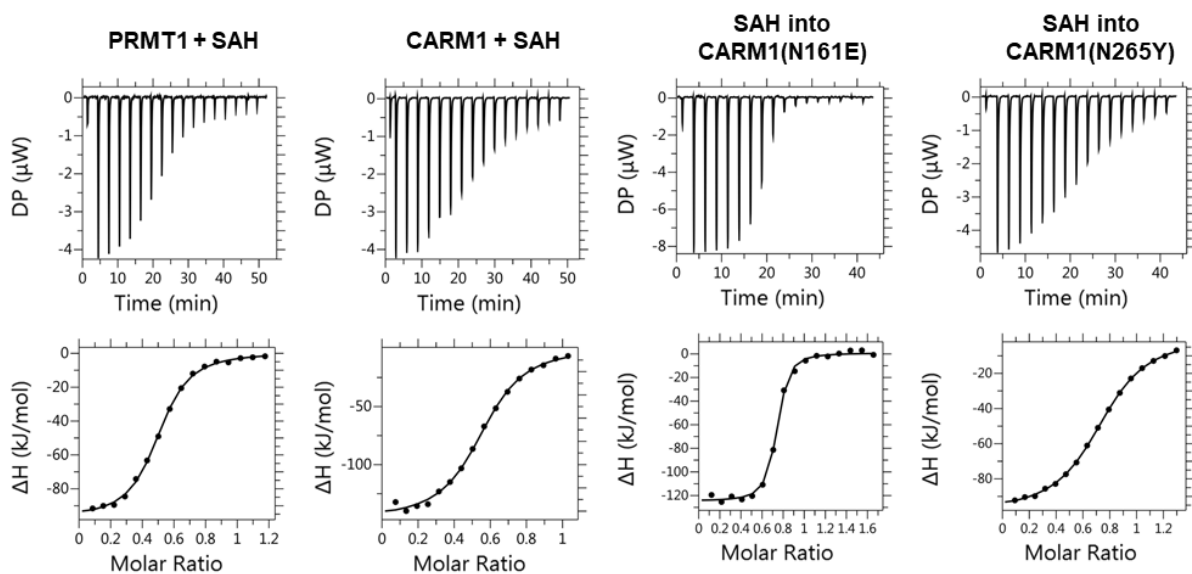
Supplementary Figure S7. ITC data for CARM1 mutants N161E and N265Y and SAH.
ITC thermograms (upper panels) and integrated heat plots (lower panels) for SAH titrations with wild-type PRMT1 and CARM1, and CARM1 mutants N161E and N265Y. The PRMT used for each titration is given above the relevant graph. Titrations were performed at 25°C with 200 μM SAH and 35 μM PRMT1. CARM1 concentrations ranged from 30–35 μM and SAH concentrations from 150 – 264 μM.
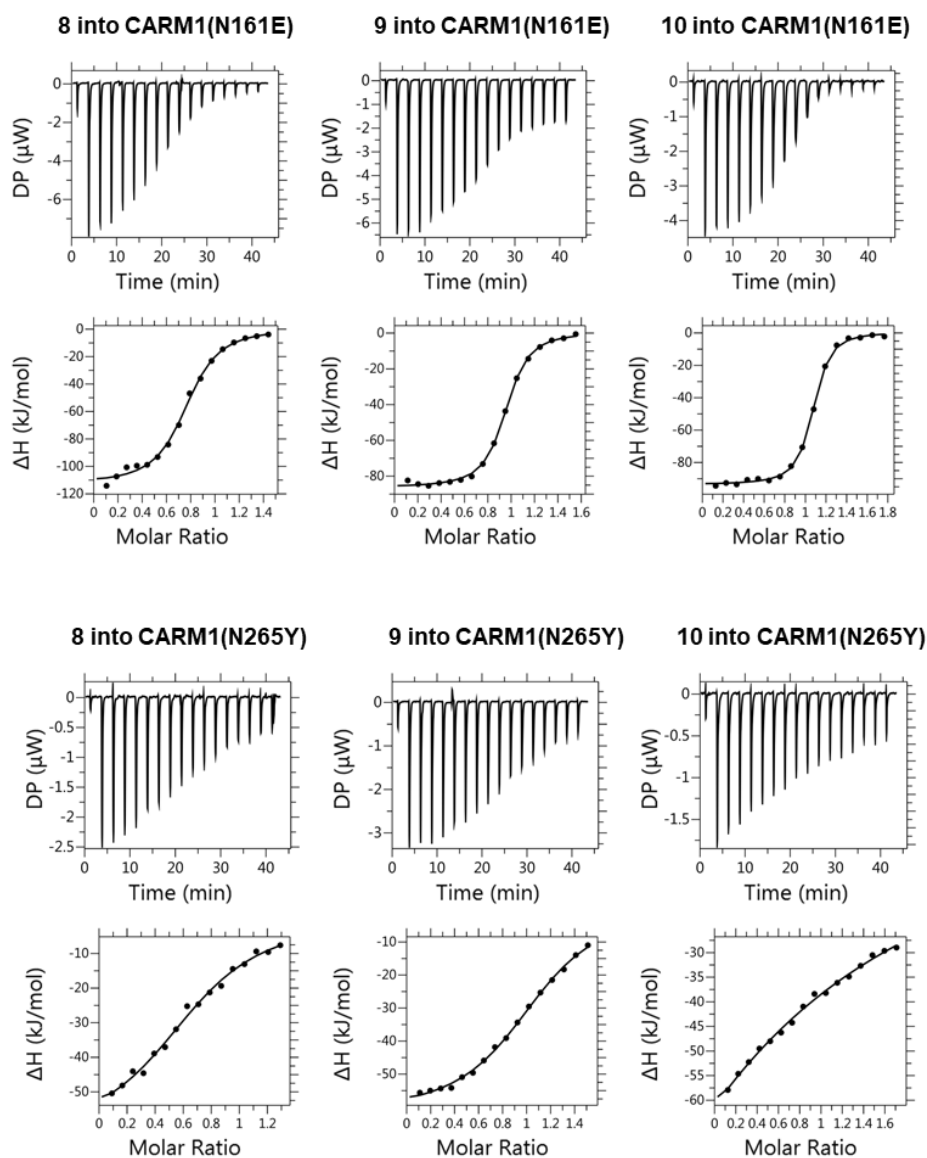
Supplementary Figure S8. ITC thermograms (upper panels) and integrated heat plots (lower panels) for inhibitors 8, 9 and 10 with CARM1 mutants N265Y and N161E.

The inhibitor and CARM1 mutant used for each titration are given above the relevant graphs. Titrations were performed at 25°C with CARM1 concentrations from $30 - 46\,\mu M$ and inhibitor concentrations from $219 - 320\,\mu M$.
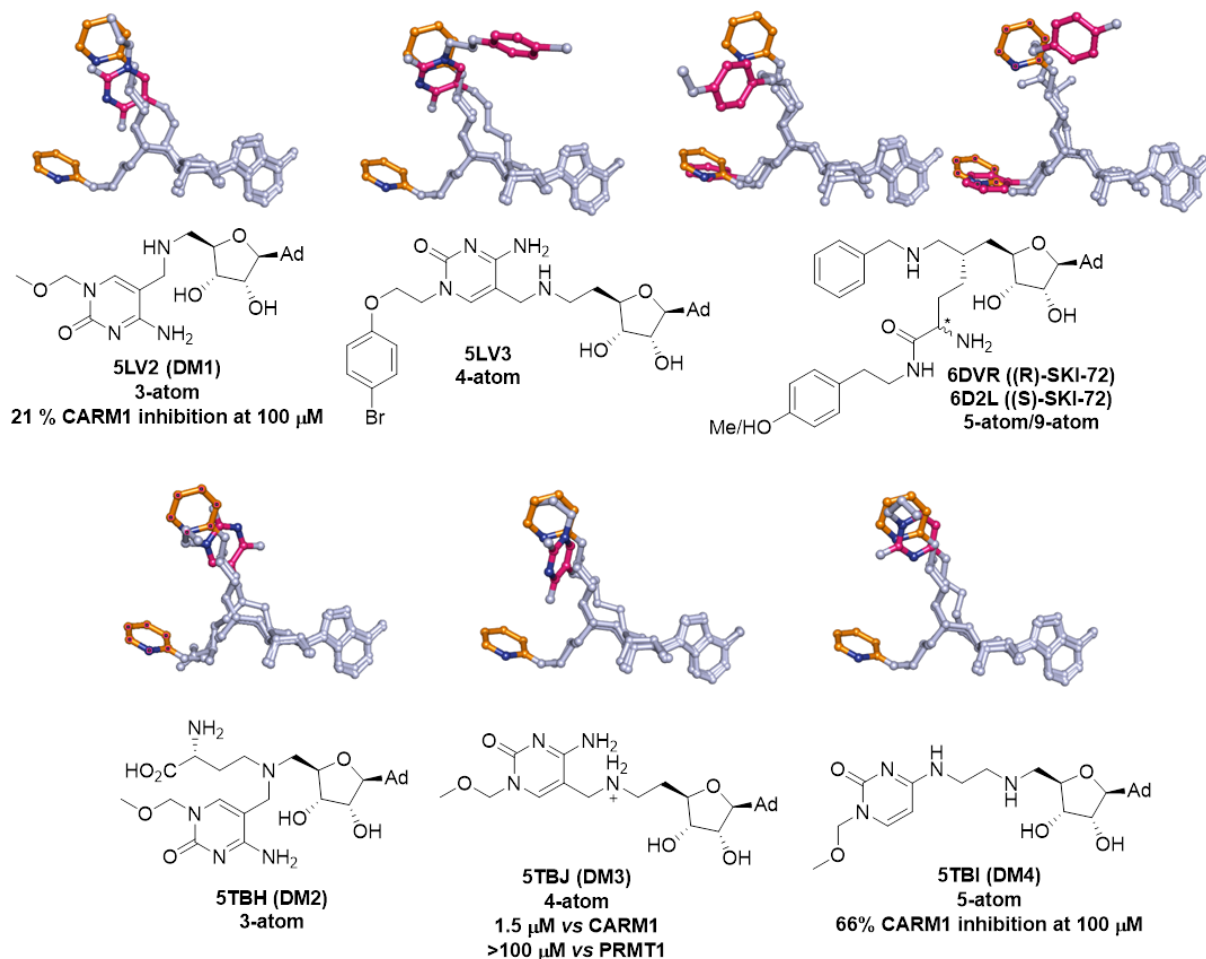
Supplementary Figure S9. Superposition of CARM1-9 complex structure with aromatic bisubstrate inhibitors co-crystallised with CARM1 in the PDB.

Ligands are shown in grey, with aromatic groups highlighted in orange (**9**) and hot pink (superposed inhibitors). Inhibitor structures, respective PDB codes and IC_{50} values (where available) are given underneath the relevant superposition. The number of atoms between the 4' adenosine carbon and the aromatic group are also indicated. The numbering of compounds DM1-DM4 is used herein and does not correspond to numbering used in the original paper.